HAL
open science

Unprotected Replication Forks Are Converted into Mitotic Sister Chromatid Bridges

Anissia Ait Saada, Ana Teixeira-Silva, Ismail Iraqui, Audrey Costes, Julien Hardy, Giulia Paoletti, Karine Fréon, Sarah Lambert, Anissia Ait Saada

To cite this version:

Anissia Ait Saada, Ana Teixeira-Silva, Ismail Iraqui, Audrey Costes, Julien Hardy, et al.. Unprotected Replication Forks Are Converted into Mitotic Sister Chromatid Bridges. Molecular Cell, 2017, 66 (3), pp.398-410.e4. 10.1016/j.molcel.2017.04.002 . hal-02331509

HAL Id: hal-02331509
https://hal.science/hal-02331509

Submitted on 29 Sep 2021

HAL is a multi-disciplinary open access archive for the deposit and dissemination of scientific research documents, whether they are published or not. The documents may come from teaching and research institutions in France or abroad, or from public or private research centers.

L'archive ouverte pluridisciplinaire **HAL**, est destinée au dépôt et à la diffusion de documents scientifiques de niveau recherche, publiés ou non, émanant des établissements d'enseignement et de recherche français ou étrangers, des laboratoires publics ou privés.

Unprotected replication forks are converted into mitotic sister chromatid bridges

Anissia Ait Saada[1,2,3], Ana Teixeira-Silva[1,2,3], Ismail Iraqui[1,2,3], Audrey Costes[1,2,3], Julien Hardy[1,2,3], Giulia Paoletti[4], Karine Fréon[1,2,3] and Sarah AE Lambert[1,2,3 *].

[1] Institut Curie, PSL Research University, CNRS, UMR3348 F-91405, Orsay, France.

[2] University Paris Sud, Paris-Saclay University, CNRS, UMR3348, F-91405, Orsay, France.

[3] Fondation Recherche Médicale team.

[4] Institut Curie, PSL Research University, CNRS, UMR144, F-75248, Paris, France.

*corresponding author: Sarah Lambert

E-mail: sarah.lambert@curie.fr

Phone: 0033 169867191

Lead contact: Sarah Lambert, sarah.lambert@curie.fr

Running title: Rad51-mediated protection of terminal forks prevents mitotic catastrophe

Keywords: Homologous recombination, aneuploidy, anaphase bridges, replication fork, genome stability.

Abstract

Replication stress and mitotic abnormalities are key features of cancer cells. Temporarily paused forks are stabilised by the intra-S phase checkpoint and protected by the association of Rad51, which prevents Mre11-dependent resection. However, if a fork becomes dysfunctional and cannot resume, such terminally-arrested forks are rescued by a converging fork to avoid unreplicated parental DNA during mitosis. Alternatively, dysfunctional forks are restarted by homologous recombination. Using fission yeast, we report that Rad52 and the DNA binding activity of Rad51, but not its strand exchange activity, act to protect terminally-arrested forks from unrestrained Exo1-nucleolytic activity. In the absence of recombination proteins, large ssDNA gaps, up to 3 kb long, occur behind terminally-arrested forks preventing efficient fork merging and leading to mitotic sister chromatid bridging. Thus, Rad52 and Rad51 prevent temporarily and terminally-arrested forks from degradation and, despite the availability of converging forks, conversion to anaphase bridges causing aneuploidy and cell death.

Introduction

The completion of eukaryotic DNA replication requires the sequential activation of replication origins and the merging of converging forks. A failure to complete DNA replication before mitosis results in the nondisjunction of sister chromatids and the formation of anaphase bridges through a variety of poorly defined mechanisms (Magdalou et al., 2014; Mankouri et al., 2013). DNA replication completion is continuously threatened by a broad spectrum of unavoidable replication fork barriers (RFBs). RFBs are caused by intrinsic chromosomal features (such as DNA sequence and chromatin), endogenous stress linked to cellular metabolism (such as transcription) and environmental factors including DNA damage (Lambert and Carr, 2013). RFBs interrupt replication fork elongation, often causing multiple temporary pauses to a single replisome and occasionally causing terminal fork arrest. To avoid these perturbations creating chromosomal aberrations, additional replication-based pathways have evolved to ensure DNA replication completion and thus genome stability maintenance.

Stressed replication forks can be either temporarily or terminally-arrested. When a fork initially slows-down or arrests, it is immediately subject to regulation by the intra-S phase checkpoint. The S-phase checkpoint acts to maintain both replisomes and fork structures in a replication-competent state, for example by limiting Exo1 nuclease activity (Berti and Vindigni, 2016; Cotta-Ramusino et al., 2005; Tsang et al., 2014). Thus, the majority of forks can resume replication after the initial blockage is resolved. In some instances, a replication fork will not be able to resume. For example, if the intra-S phase checkpoint fails, replication forks become dysfunctional and eventually terminally-arrested; such forks referring to as collapsed forks. To accommodate the problems caused by replication stress, cells thus exploit several mechanisms to ensure replication is completed in a timely manner (Berti and Vindigni, 2016). First, eukaryotic genomes contain a large excess of replication origins which buffer the consequences of fork arrest: a converging fork can arise from an adjacent dormant origin and merge with an arrested fork (Blow et al., 2011; Ge et al., 2007; Kawabata et al., 2011; Sabatinos et al., 2015; Woodward et al., 2006). Alternatively, when a converging fork is not timely available, terminally-arrested forks can be reactivated by DNA repair pathways such as homologous recombination (HR). These compensatory mechanisms are crucial for cellular resistance to replication stress and prevent the persistence of unreplicated parental DNA into mitosis.

When replication is perturbed experimentally, the mitotic consequences are expressed most obviously at common fragile sites (CFSs). CFSs were initially defined as genomic loci prone to chromosome breakage when cells are exposed to mild replication stress (Glover et al., 1984). CFSs have subsequently been shown to be hotspots for chromosomal rearrangement in cancer cells (Le Tallec et al., 2011; Le Tallec et al., 2013). Many CFSs replicate late in S-phase and it has been

85 demonstrated that their replication can be further delayed by mild replication stress (Debatisse et al.,
86 2012). To date, it has not been possible to define a common cause for all fragile sites. Recent models
87 suggest that CFS instability results from paucity of replication origins combined with difficult to
88 replicate features such as refractory DNA sequences or extremely long transcriptional units (Helmrich
89 et al., 2011; Letessier et al., 2011; Ozeri-Galai et al., 2011). In this interpretation, CFS loci cannot
90 compensate for temporarily paused or terminally-arrested forks by activating dormant origins. Thus,
91 cells are prone to enter mitosis with partially replicated DNA at these loci (Debatisse et al., 2012;
92 Mankouri et al., 2013). Attempting mitosis with unreplicated DNA regions results in the formation of
93 ultrafine bridges (UFBs) during anaphase (Chan et al., 2009; Naim and Rosselli, 2009). UFBs consist of
94 stretched DNA structures coated with PICH (Plk1-interaction checkpoint helicase) and the single-
95 stranded DNA protein RPA (replication protein A) (Chan et al., 2007). Thus, replication-stress induced
96 UFBs are thought to contain ssDNA originating from incomplete replication of CFSs. UFBs-like
97 structures have been also described in yeast models, as a consequence of disturbed DNA replication
98 (Germann et al., 2014; Sabatinos et al., 2015; Sofueva et al., 2011).

99 Maintaining replication fidelity relies on close links between the replication machinery and HR. The
100 core of HR is the Rad51 recombinase, which forms filaments on ssDNA and mediates invasion of the
101 ssDNA into a homologous duplex. In yeasts, Rad51 association with ssDNA requires the Rad52 loader,
102 while in mammalian cells, this role is primarily performed by the tumour suppressor BRCA2 (Costes
103 and Lambert, 2013). Historically, HR has been studied in the context of double strand break (DSB)
104 repair but, more recently, HR proteins have been shown to play critical roles in maintaining genome
105 integrity during DNA replication; these replicative functions being independent of DSB repair (Carr
106 and Lambert, 2013; Petermann et al., 2010; Schlacher et al., 2011). HR proteins contribute to the
107 robustness of DNA replication in several ways: 1) BRCA2, Rad52 and Rad51 protect nascent strands
108 of stalled forks, checkpoint-stabilised, from Mre11-dependent resection (Hashimoto et al., 2010;
109 Higgs et al., 2015; Schlacher et al., 2011); 2) in some circumstances, Rad51 participates in the
110 remodelling of stressed forks to promote fork reversal, a process that is proposed to promote DNA
111 lesions bypass or replication resumption (Zellweger et al., 2015); 3) when forks become
112 dysfunctional, HR proteins restart forks that likely results in the construction of a new replisome
113 (Hashimoto et al., 2011; Iraqui et al., 2012; Miyabe et al., 2015; Mizuno et al., 2013; Petermann et al.,
114 2010).

115 Using a site-specific RFB in fission yeast, we followed *in vivo* the fate of a single terminally-arrested
116 fork in the absence of HR. Contrary to our expectations, we found that, despite the apparent
117 progression of converging forks, this single terminally-arrested fork is converted into an anaphase
118 bridge resembling a UFB. We show that the binding of Rad51, but not its strand exchange activity, is

119 required to restrict Exo1-mediated fork resection. This function is independent of the previously
120 described roles for Rad51 in replication fork restart. We further demonstrate that the excess ssDNA
121 at terminally-arrested forks is the cause of sister chromatid bridging which subsequently results in
122 aneuploidy. We propose that the merging of a converging fork with an unprotected terminally-
123 arrested fork results in termination failure and subsequent UFB formation during mitosis. Our data
124 reveal a new role for Rad51-mediated fork-protection that ensures the rescue of arrested forks by an
125 incoming converging fork.
126
127
128
129
130
131
132
133
134
135
136
137
138
139
140
141
142
143
144

145 **Results**

146 To assess the role of arrested forks in replication stress-induced mitotic abnormalities, we exploited a
147 conditional RFB, *RTS1*, to block the replisome in a polar manner at a defined locus (Figure 1A and
148 Figure S1A). In the *RTS1* system, fork arrest is mediated by the *RTS1*-bound protein Rtf1, the
149 expression of which is regulated by the *nmt41* promoter. Rtf1 induction results in >90 % of forks
150 becoming blocked at the *RTS1*-RFB (Lambert et al., 2005). Arrested forks are resolved by a converging
151 fork or restarted by HR within 20 minutes (Miyabe et al., 2015; Nguyen et al., 2015). Restart occurs
152 through the generation of a ssDNA gap, which is subsequently coated with Rad51 recombinase
153 (through its loader Rad52) which, following strand invasion, restarts replication (Mizuno et al., 2013;
154 Tsang et al., 2014). The restarted replisome is associated to a non-processive DNA synthesis, with
155 polymerase delta replicating both strands, and is thus likely mechanistically different from an
156 unperturbed replisome and insensitive to the RFB (Miyabe et al., 2015). In the absence of either
157 Rad52 or Rad51, forks arrested at the *RTS1*-RFB cannot restart and thus remain irreversibly arrested
158 (Lambert et al., 2010; Mizuno et al., 2009).

159

160 **Rad52 prevents a single terminally-arrested fork generating an anaphase bridge and aneuploidy**

161 We have previously demonstrated that the *t>ura4<ori* construct blocks the two replisomes
162 converging on the *ura4* locus (*t*= telomere proximal; chevrons represent the presence and
163 directionality of the *RTS1* barrier; *ori* indicates the location of the closest origin). Wildtype (*wt*) cells
164 overcome the potential inability to replicate the 1.7 Kb *ura4* locus by restarting one or both forks via
165 HR. Because the two *RTS1* sequences are present in an inverted orientation on either side of *ura4*,
166 occasional erroneous (ectopic) strand invasion events result in aberrant chromosome configurations:
167 specifically acentric and dicentric chromosomes (Lambert et al., 2010; Mizuno et al., 2009).
168 Visualizing mitosis in these cells reveals abnormal chromosome segregation events expected from
169 dicentric chromosome segregation (Figure S1). Our initial expectation was thus that, when HR was
170 prevented by the deletion of *rad52*, acentric/dicentric chromosomes would not be present and thus
171 these structural mitotic abnormalities would be lost. However, in *rad52-d* cells, we still observed
172 DNA bridges with multiple discontinuities, suggesting breakage, and uneven segregation of nuclei,
173 resulting in aneuploidy (Figure S1).

174 In *rad51-d* or *rad52-d* cells, replication cannot restart from blocked replisomes (Iraqui et al., 2012;
175 Lambert et al., 2010). Thus, mitotic defects presumably reflect the persistence of unreplicated
176 parental DNA at the *ura4* locus when cells enter mitosis, a situation reminiscent of human CFSs.
177 Therefore, our prediction was that, if replication could be completed by a converging fork, the
178 remaining single terminally-arrested fork would not prevent the completion of replication and

179 correct mitotic segregation would be restored. To allow the fork moving towards the centromere to
180 reach the terminally-arrested fork at the centromere-proximal *RTS1*-RFB, the telomere-proximal
181 *RTS1*-RFB was deleted (*t-ura4<ori* locus) (Figure S1A). Surprisingly, mitotic abnormalities, including
182 discontinuous DNA bridges, were still observed in both *rad52-d* and *rad51-d* cells, whereas these
183 defects were not present in *wt* cells, in which acentric/dicentric chromosomes no longer formed
184 (Figure S1C).
185
186 **Dynamic of anaphase bridges containing the active *RTS1*-RFB**

187 To investigate whether the mitotic bridges contained the active RFB site, we integrated a *lacO* array
188 telomere-proximal to the RFB (*t-LacO-ura<ori*, Figure 1A). We tracked the fate of the single
189 terminally-arrested fork locus *in vivo* by visualizing *LacO*-bound GFP-LacI. Because LacI binding to
190 *LacO* arrays can impede fork progression, we exploited a LacI variant with which fork perturbation is
191 avoided but LacI foci can be detected (Dubarry et al., 2011). In the absence of an active *RTS1*-RFB,
192 *LacO* mitotic bridges were observed in <2% of *wt* and *rad52-d* cells. Thus, LacI binding had a minimal
193 impact on fork progression (Figure 1B). In contrast, *RTS1*-RFB induction resulted in the formation of
194 mitotic *LacO*-positive bridges in ~ 20% of post-mitotic cells, in *rad52-d* but not *wt* cells (Figure 1B, top
195 panel). Thus, mitotic bridges contain the site of fork arrest surrounded by dsDNA. A proportion of the
196 *LacO*-bridges were long-lived, persisting through cytokinesis (Figure 1B, middle panel). Interestingly,
197 ~ 14% of post-mitotic cells displayed uneven LacI focus segregation in *rad52-d* cells, suggesting
198 breakage of *LacO*-bridges (Figure 1B, bottom left panel).

199 We confirmed that a converging fork could reach the terminally-arrested fork at the *RTS1*-RFB by
200 monitoring the duplication of the *LacO* arrays by analyzing single and sister LacI-foci in G2 cells
201 (Figure 1C-D). Similar frequencies of sister LacI-foci were observed regardless of RFB activity and HR
202 status. Thus, *LacO*-bridges resulting from terminally-arrested forks were not a consequence of the
203 failed progression of converging forks. Thus, Rad52 prevents the aberrant segregation of a replication
204 stress site and ensures its balanced transmission to daughter cells.

205 To investigate the dynamics of *LacO*-bridge formation and resolution, we performed time-lapse
206 microscopy. In *wt* cells, *LacO*-bridges were transient and resolved within 10 minutes of anaphase
207 onset (Figure 2A-B). This rapid dynamics likely accounts for low levels of *LacO*-bridges as observed by
208 snapshot microscopy. Furthermore, the *t-LacO-ura<ori* locus is ~700 kb from the rDNA locus and the
209 *LacO*-bridges in *wt* cells may thus reflect the late mitotic segregation of rDNA units (Granot and
210 Snyder, 1991; Win et al., 2005). In contrast, in *rad52-d* cells, ~90% of anaphases displayed a *LacO*-
211 bridge with 67% of these remaining unresolved 10 minutes after anaphase onset. Analysis of

212 individual *LacO*-bridges showed that ~20% broke either before or at the onset of cytokinesis (Figure
213 2B-C, Figure S2A and movie 1).

214 GFP-LacI binds *LacO*-arrays when double stranded. We tried to stain *LacO*-bridges with DNA dye.
215 Surprisingly, stretched *LacO*-bridges were not positively stained with Hoechst whereas broken *LacO*-
216 bridges showed positive Hoechst staining (Figure S2B). Possibly, *LacO*-arrays are refractory to DNA
217 dye staining because of stretching which is relaxed when bridges break. Thus, the discontinuous
218 bridges observed by Dapi staining were likely broken bridges (Figure S1).

219 We conclude that, without Rad52, a single terminally-arrested fork is converted into an anaphase
220 bridge, resembling human UFB, which often breaks during mitosis. This occurs despite the availability
221 of converging forks and an apparent absence of unreplicated parental DNA downstream from the
222 site of replication stress.

223

224 **Rad52 protects the integrity of arrested forks by restricting Exo1 activity**

225 To determine the integrity of forks terminally-arrested, we defined the extent of ssDNA exposed in
226 the vicinity of the *RTS1-RFB*. We have previously shown that replication restart at the *RTS1*-RFB is not
227 initiated by a DSB but by a ssDNA gap formed in an Exo1-dependent, and Mre11 nuclease activity-
228 independent manner (Figure 3A) (Tsang et al., 2014). Consistent with this, RPA recruitment extended
229 ~1 kb upstream from the arrested fork and RPA recruitment was significantly reduced in *exo1-d* cells.
230 (Figure 3B, blue and black lines). When Rad52 was deleted, RPA recruitment extended further
231 upstream from the *RTS1*-RFB (>3kb), suggesting an accumulation of ssDNA compared to *wt* (Figure
232 3B, red line). Importantly, the excess RPA recruitment in *rad52-d* cells occurred exclusively upstream
233 from the site of fork arrest. Using a qPCR assay to directly monitor ssDNA, we confirmed that excess
234 RPA recruitment reflected the accumulation of ssDNA (Figure 3C). In *wt* cells, ssDNA was enriched
235 110 and 450 bp upstream from the *RTS1*-RFB, but no enrichment above background levels (RFB OFF
236 condition) was observed at 1.8 and 2.2 kb. Consistent with the RPA ChIP data, ssDNA enrichment at
237 450 bp, but not at 110 bp, was Exo1-dependent. This suggests that additional nucleases are able to
238 generate small ssDNA gaps at terminally-arrested forks. Due to technical problems related to primer
239 design and efficiency, we were unable to assess ssDNA amount between 450 bp and 1.8 kb. In the
240 absence of Rad52, the enrichment in ssDNA was clearly observed 1.8 and 2.2 kb upstream from the
241 *RTS1*-RFB. The difference in ssDNA accumulation between *wt* and *rad52-d* cells was specific to the
242 active *RTS1*-RFB, since no significant differences were observed at the control locus (Figure 3C).

243 To establish that ssDNA enrichment corresponded to arrested replication forks containing large
244 ssDNA gaps, we analyzed replication intermediates using two-dimensional gel electrophoresis

245 (2DGE). A tail emanating from the fork-arrest signal and descending towards the linear arc was
246 observed in *wt* cells and was absent in *exo1-d* cells (Figure 3D-F). Alkaline 2DGE confirmed that this
247 tail signal corresponded to Exo1-mediated resection of newly replicated strands (Figure S3A-B). Thus,
248 this replication intermediate was generated by the resection of unbroken forks. Consistent with the
249 RPA ChIP and ssDNA enrichment assays, more resected forks were present in *rad52-d* cells (Figure
250 3E-F). Thus, Rad52 has the replication-specific function of limiting resection of nascent DNA at
251 terminally-arrested forks, primarily by restricting the formation of large ssDNA gaps. This terminal
252 fork protection function of Rad52 likely allows replication termination, thus preventing subsequent
253 anaphase bridges formation and chromosome breakage. Taken together, our data suggest that the
254 progression of a converging fork towards an unprotected terminally-arrested fork creates failure in
255 termination, which cannot be resolved before the onset of mitosis.
256

257 **Failed merging of unprotected terminally-arrested and converging forks drives mitotic sister**
258 **chromatid bridging**

259 If converging forks cannot effectively merge with unprotected terminally-arrested forks, large ssDNA
260 gaps at such forks should persist into mitosis and correlate with *LacO*-bridges formation. We used
261 fluorescence microscopy to monitor RPA recruitment to the *RTS1*-RFB during cell cycle. GFP-LacI and
262 RPA focus mark dsDNA downstream and ssDNA upstream from the RFB, respectively. A RPA focus is
263 thus expected adjacent or in close proximity to a GFP-LacI focus. We considered RPA being recruited
264 to the *RTS1*-RFB when a RPA focus is touching or merging fully or partially a GFP-LacI focus (Figure 4A
265 and Figure S4A). In *wt* cells, RPA was transiently recruited to active RFBs in S-phase cells, in an Exo1-
266 dependent manner, and then evicted in G2 cells (Figure 4A-B). We interpret this as reflecting
267 transient RPA recruitment to resected forks, followed by efficient replication restart or merging with
268 the converging fork. Without Rad52, we observed an increased number of cells showing RPA
269 recruitment to active RFBs, in S and G2 phase. This is consistent with ssDNA gaps at terminally-
270 arrested forks remaining unrepaired during the transition from S to G2 phase. Furthermore, >90% of
271 mitotic *LacO*-bridges were positively stained for RPA, consistent with RPA recruited in S-phase
272 remaining associated with large ssDNA gaps at terminally-arrested forks when cells enter mitosis
273 (Figure 4C and Figure S4B).

274 We followed the dynamic RPA recruitment to terminally-arrested forks by time-lapse microscopy.
275 ~50% of *LacO*-bridges arose in cells in which RPA and LacI were co-recruited in the preceding G2
276 phase. Furthermore, ~60% of *LacO*-bridges arose in cells which displayed RPA foci at the nexus of the
277 two nuclei in early anaphase (with or without merging with a LacI focus) (Figure 4E-F and Figure S4
278 and movie 2). We conclude that UFB-like *LacO*-bridges result from and contain unprotected

279 terminally-arrested forks. Thus, terminally-arrested forks, that are not protected by Rad52, are
280 subsequently converted into UFB-like structures in mitosis.

281 In most cases, RPA staining of anaphase bridges was symmetric, covering almost all *LacO*-bridges
282 (Figure 4C and Figure S4B). This suggests that both sister chromatids had undergone resection
283 upstream from the RFB and remain physically associated in mitosis. Thus, *LacO*-bridges are
284 apparently formed of unresolved intertwined sister chromatid: each chromatid contains dsDNA
285 marked by *LacO*-arrays and ssDNA marked by RPA (Figure 4F). Our data indicate that converging
286 forks are able to reach unprotected forks, with an apparent absence of unreplicated parental DNA
287 downstream from the RFB. Thus, we propose that intertwined sister chromatid arise from
288 termination failure rather than failure in completing replication. Furthermore, Hoechst staining failed
289 to detectably stain telomere-proximal regions at the metaphase plan in mitosis showing *LacO*-
290 bridges (Figure S2B). Altogether, our data suggest that unprotected terminally arrested-fork cannot
291 merge accurately with converging fork. This failure in fork merging results in intertwined sister
292 chromatid resembling UFBs.
293

294 **Excess ssDNA at terminally-arrested forks causes lethal UFBs and enhanced genetic instability**

295 We asked whether excess ssDNA is responsible for termination failure. We reported that Rad52
296 recruitment to the *RTS1*-RFB requires the MRN complex (Tsang et al., 2014). We analyzed the
297 resection of terminally-arrested forks in the *rad52-d rad50-d* double mutant and found that the lack
298 of Rad50 was not sufficient to fully abolished fork-resection (Figure S3C). We thus focus on the role
299 of Exo1.

300 The deletion of *exo1* in *rad52-d* cells was sufficient to alleviate extended RPA recruitment, ssDNA
301 formation upstream from the active *RTS1*-RFB and fully abolished fork-resection (Figure 3B, green
302 line and C-F). Consistent with this, RPA foci were not co-recruited to the *RTS1*-RFB in either S or G2-
303 phase in *exo1-d rad52-d* cells (Figure 4B). Surprisingly, the short ssDNA gaps of less than 450 bp that
304 are not Exo1-dependent in *wt* cells were not observed in *rad52-d exo1-d* cells (Figure 3B-C). Our
305 interpretation of this is that Rad52-dependent HR processes restrict Exo1 activity at terminally-
306 arrested forks, while also acting to promote limited resection by additional nucleases. Thus, the
307 absence of Exo1 restores the integrity of terminally-arrested forks, although they remain unable to
308 restart replication. If the RPA-coated ssDNA gaps at terminally-arrested forks are responsible for
309 sister chromatid non-disjunction, concomitant *rad52* and *exo1* deletion should be sufficient to
310 alleviate the formation of UFB-like structures.

311 The high frequency of UFB-like structures (mitotic *LacO*-bridges) observed upon activation of the
312 *RTS1*-RFB was greatly reduced in double mutant cells (Figure 5A, left panel), confirming the
313 interdependency of ssDNA gaps and subsequent anaphase bridges formation. This suppression effect
314 did not result from an inability of cells to enter mitosis (Figure S3D). Interestingly, the unbalanced
315 segregation of LacI foci observed in *rad52-d* cells, while also decreased upon concomitant *exo1*
316 deletion, was reduced by only 34% (Figure 5A, right panel). Thus, terminally-arrested forks, even if
317 protected against Exo1 activity, remain unstable. We tested the genetic instability of *ura4*$^{+}$, located
318 upstream from the RFB. Loss of *rad52* resulted in an increase RFB-dependent rate of *ura4* loss which
319 was relieved by the concomitant loss of Exo1 (Figure 5B-C). Thus, excess RPA-coated ssDNA at
320 stressed forks is responsible for sister chromatid nondisjunction and elevated genetic instability,
321 immediately upstream from the site of fork arrest. We also observed that activation of the *RTS1*-RFB
322 decreased the viability of *rad52-d* cells and that this loss of viability was rescued by deleting *exo1*
323 (Figure 5D). These data indicate that pathological termination between unprotected terminally-
324 arrested forks and converging forks result in lethal UFB-like structures which contribute to genomic
325 instability.
326
327 **Rad51 binding activity is sufficient to prevent pathological termination at terminally-arrested forks**

328 Our data, together with previously published work, suggest that dysfunctional forks can either be
329 rescued by a converging fork or restarted. Both processes require Rad52. To investigate the
330 interdependence of fork-protection and fork-restart functions, we replaced *rad51*$^{+}$ with the mutated
331 *rad51-3A* form (R152A-R324A-K334A). The mutant protein can bind ssDNA and dsDNA, form stable
332 nucleoprotein filaments on ssDNA, but cannot perform the strand exchange reaction (Cloud et al.,
333 2012). Rad51-3A was expressed to the same level as Rad51 (Figure S5A). *rad51-3A* cells were
334 defective for spontaneous gene conversion and were equally sensitive to bleomycin and MMS
335 treatments, as *rad51-d* cells (Figure 6A and Figure S5B-C). Rad51-3A formed foci in response to MMS
336 and was recruited to the active *RTS1*-RFB, similarly to Rad51 (Figure S5D-E).

337 To investigate the impact of Rad51-3A on replication restart, we exploited a reporter gene (*ura4-*
338 *sd20*) (Iraqui et al., 2012). In this assay, the *ura4-sd20* allele is downstream from the *RTS1*-RFB and
339 can be used to monitor the frequency of forks restarted at the *RTS1*-RFB based on the restoration of
340 a functional *ura4* gene (Figure 6B). The effectiveness of replication slippage was decreased by ~60%
341 in both *rad51-3A* and *rad51-d* cells, demonstrating the requirement of Rad51 strand-exchange
342 activity to promote fork restart (Figure 6C). Thus, Rad51 foci can occur in response to replication
343 stress, without effective homologous recombination event at the site of fork arrest.

344 To investigate the impact of Rad51-3A on fork-protection, we utilized the 2DGE resection assay
345 described in figure 3E, the frequency of *LacO*-bridge and the uneven segregation of the *LacO* locus.
346 As previously observed for *rad52-d* cells, terminally-arrested forks were extensively resected and
347 converted into UFB-like structures in the absence of Rad51 (Figure 6D-E). Thus, fork protection to
348 prevent pathological termination requires both the recombinase Rad51 and its loader Rad52. In
349 contrast, cells expressing Rad51-3A displayed none of these pathological features upon activation of
350 the *RTS1*-RFB, demonstrating the requirement of Rad51 binding activity, but not its strand-exchange
351 activity, for fork-protection (Figure 6D-E). Thus, extensive degradation of terminally-arrested forks in
352 the absence of Rad52/Rad51 proteins is not simply a consequence of defective fork restart: the role
353 of Rad51 in protecting terminally-arrested replication forks is genetically separable from its function
354 in restarting forks.
355
356
357
358
359
360
361
362
363
364
365
366
367
368
369
370

371 **Discussion**

372 The resolution of replication stress is vital to suppress a wide range of tumor-initiating events
373 including mis-segregation of chromosomes during mitosis. Rad51-mediated recombination processes
374 at replication forks have been shown to be central to this. Global alteration of fork progression
375 previously identified a role for HR proteins at temporarily arrested forks through fork remodeling and
376 prevention from Mre11 or Dna2-dependent resection of nascent strands (Hashimoto et al., 2010;
377 Higgs et al., 2015; Schlacher et al., 2011; Schlacher et al., 2012; Zellweger et al., 2015). By studying a
378 well-controlled site-specific RFB, we had previously characterized a separate role for Rad51 in
379 promoting HR-mediated restart of dysfunctional forks (Lambert et al., 2010; Miyabe et al., 2015).
380 Here, by following the fate *in vivo* of the *RTS1*-RFB, we have revealed a novel link between replication
381 arrest and mitotic mis-segregation events. Our main unexpected findings are: 1) terminally-arrested
382 forks require Rad52/Rad51-mediated fork protection if they are to be resolved by the arrival of a
383 converging fork (Figure 7, left panel); 2) If terminally-arrested forks are not protected by
384 Rad52/Rad51, fork merging fails. The result is manifested in mitosis as an anaphase bridge (Figure 7,
385 right panel). Mechanistically, we demonstrate that Rad51 DNA binding, but not Rad51 strand-
386 exchange activity, is required for terminally-arrested fork protection. Loss of Rad51 DNA association
387 results in excess Exo1-dependent ssDNA formation upstream from the site of terminal fork arrest.
388 This excess of ssDNA causes the subsequent conversion of the unprotected fork into a UFB-like
389 structure that is further damaged as cells progress through mitosis.
390

391 **Rad52/Rad51 restrict Exo1 activity at terminally-arrested forks in a recombination-independent**
392 **manner**

393 Temporarily-arrested forks are subject to regulation by the intra-S phase checkpoint which includes
394 the nucleolytic processing of nascent strands and architectural changes, such as fork reversal, to
395 facilitate the resumption of replication (Berti and Vindigni, 2016). However, uncontrolled resection at
396 these stably stalled forks is detrimental to genome stability. Recombination factors (Rad52 and
397 Rad51 in yeasts; BRCA2 and FANCD2 in higher eukaryotes) prevent excessive nascent strand
398 degradation at forks that have been temporarily stalled by hydroxyurea (HU) or damaged by methyl-
399 methane sulfonate (MMS) treatment. DNA fiber-based approaches and analyses of fork structures by
400 electronic microscopy have demonstrated that uncontrolled resection (~1.8 kb/hour) generates
401 short gaps (<300 nt) both close to and further away from the fork junction (Hashimoto et al., 2010;
402 Higgs et al., 2015; Schlacher et al., 2011; Schlacher et al., 2012).

403 If replication forks are not stabilized by the intra-S phase checkpoint, they become dysfunctional.
404 Such forks cannot simply resume replication and must either be resolved by an incoming converging

405 fork or, if this does not occur in a timely manner, be restarted by the action of HR. Using an allele of
406 *rad51* that cannot initiate strand exchange, but able to bind DNA, we have separated the function of
407 Rad51 in terminally-arrested forks restart from a new function in protecting terminally-arrested forks
408 from excessive Exo1-dependent nascent strand degradation. While restart of dysfunctional forks
409 requires the strand exchange functions of Rad51, fork-protection depends only on the initial
410 association of Rad51 with DNA. Given the potential deleterious outcomes of Rad51-mediated fork
411 repair and restart on genome stability, our data suggest that protection and restart of dysfunctional
412 forks are separate Rad51 functions with different requirements for the maintenance of genome
413 stability (Carr and Lambert, 2013).
414
415 **Unprotected forks are converted into anaphase bridges**

416 A second important observation we made was that a terminally-arrested replication fork, which is
417 not protected from Exo1-dependent resection by Rad52/Rad51, cannot effectively merge with a
418 converging fork. The consequence of this failed merger is the formation in the subsequent mitosis of
419 a sister chromosome bridge that resembles the structure of a UFB: two intertwined sister chromatids
420 harboring dsDNA and ssDNA (Figure 7, right panel). Since these bridges arise at site of fork arrest, we
421 equate them to a potential subset of UFBs that characterize human CFS. In yeasts and mammals, the
422 induction of artificial bidirectional fork barriers (*LacO* arrays bound by the repressor LacI) results in
423 UFBs formation, further supporting a scenario in which the irreversible arrest of converging
424 replisomes results in the persistence of unreplicated parental DNA, generating UFB in mitosis (Beuzer
425 et al., 2014; Germann et al., 2014; Jacome and Fernandez-Capetillo, 2011; Sofueva et al., 2011).
426 While our data do not rule out this hypothesis, we speculate that the bridges we observe here may
427 reflect a novel route to the formation of UFBs. This would be consistent with observations in human
428 cells that RAD51 is required to prevent CFS instability and the formation of anaphase bridges,
429 including PICH-positive UFBs (Laulier et al., 2011; Schwartz et al., 2005; Wilhelm et al., 2014).

430 Our data suggest that the progression of unperturbed converging forks towards an unprotected
431 terminally-arrested fork results in a pathological termination event, the exact nature of which
432 remains to be determined. However, in considering the potential nature of such events, it is of note
433 that replication termination has recently been proposed to occur when the CMG helicase
434 (CDC45/MCM2-7/GINS) of one replisome encircles dsDNA from the lagging strand of the adjacent
435 converging replicon (Dewar et al., 2015). If unprotected forks have excessive ssDNA gaps, the CMG
436 helicase of the converging replisome may encounter difficulties in reaching the dsDNA. Possibly,
437 concatenation or premature condensation of ssDNA may also challenge topoisomerase activity and
438 compromise fork merging.

439 **The rescue of terminally-arrested forks by origin firing requires Rad51-mediated fork protection**

440 We have revealed a previously unknown role for Rad52/Rad51-mediated fork protection in
441 preventing sister chromatid bridging at replication stress site. Our data reveal that terminally
442 arrested forks can be rescued through the firing of dormant origins only in the presence of Rad51
443 binding and, thus, fork-protection. We previously reported the frequent formation of Rad52 and
444 Rad51 foci in both S and G2 phases, following RFB activation (Lambert et al., 2005). Using an
445 analogous RFB, Nguyen *et al*. recently showed that Rad52 remains associated with arrested forks at
446 the time point at which fork merging probably occurs (Nguyen et al., 2015). These observations
447 suggest a time-window for the association of Rad52/Rad51 with dysfunctional forks exceeding the
448 ~20 minutes required for successful replication restart (Miyabe et al., 2015). We suggest that
449 Rad51/Rad52 facilitates accurate termination at sites of prolonged fork arrest, as well as offering the
450 potential to restart the fork, should an incoming converging, fork fail to appear at a timely manner.

451 Replication stress and structural mitotic abnormalities are common features of cancer cells. By
452 showing that unprotected dysfunctional forks drive the formation of UFB-like structures, mitotic
453 chromosome breakage and aneuploidy, we have established a novel genome instability pathway
454 linking replication stress and mitotic defects. We suggest that unprotected fork-associated mitotic
455 defects contribute to the genomic instability of neoplastic lesions early in cancer development.
456
457
458
459
460
461
462
463
464
465
466
467

468 **Author contributions:** A.A.S, A.T.S, I.I., A.C. J. H. and K.F. performed the experiments. A.A.S., A.T.S.
469 and S.A.E.L. contributed to experimental design and data analysis. A.A.S. and S.A.E.L. wrote the
470 manuscript.
471

472 **Acknowledgements**: We thank P. Pasero, B. Lopez and AM Carr for critical reading of the manuscript
473 and helpful discussions. We thank the laboratory of A. Paoletti (Institut Curie, Paris) for assistance
474 with time-lapse microscopy. We also thank the PICT-IBiSA@Orsay Imaging Facility of the Institut
475 Curie. None of the authors of this manuscript have a financial interest related to this work.
476

477 **Financial disclosure:** AAS, ATS, AC and II were funded by a French governmental fellowship, the
478 Institut Curie international PhD program, *Association pour la Recherche sur le Cancer* (ARC), and the
479 *Fondation pour la Recherche Medicale* (FRM), respectively. This work was supported by the Institut
480 Curie, the CNRS, the *fondation ARC*, the *Ligue* (*comité Essone*), *l'Agence Nationale de la Recherche*
481 ANR-14-CE10-0010-01, the *Institut National du Cancer* INCA 2013-1-PLBIO-14, and the *Fondation*
482 *pour la Recherche Médicale* "Equipe FRM DEQ20160334889". The funders had no role in study
483 design, data collection and analysis, the decision to publish, or preparation of the manuscript.
484
485
486
487
488
489

490 **Supplemental items**

491 **Movie 1:** Time-lapse movie of *LacO*-bridges breaking at cytokinesis (related to Figure 1).

492 **Movie 2:** Time-lapse movie of RPA-positive *LacO*-bridge showing RPA being recruited to the RFB in
493 the previous G2 phase (related to Figure 4).
494
495
496

497 **References**

498 Berti, M., and Vindigni, A. (2016). Replication stress: getting back on track. Nature structural &
499 molecular biology *23*, 103-109.
500 Beuzer, P., Quivy, J.P., and Almouzni, G. (2014). Establishment of a replication fork barrier following
501 induction of DNA binding in mammalian cells. Cell cycle *13*, 1607-1616.
502 Blow, J.J., Ge, X.Q., and Jackson, D.A. (2011). How dormant origins promote complete genome
503 replication. Trends in biochemical sciences *36*, 405-414.
504 Brewer, B.J., Lockshon, D., and Fangman, W.L. (1992). The arrest of replication forks in the rDNA of
505 yeast occurs independently of transcription. Cell *71*, 267-276.
506 Carr, A.M., and Lambert, S. (2013). Replication stress-induced genome instability: the dark side of
507 replication maintenance by homologous recombination. Journal of molecular biology *425*, 4733-
508 4744.
509 Chan, K.L., North, P.S., and Hickson, I.D. (2007). BLM is required for faithful chromosome segregation
510 and its localization defines a class of ultrafine anaphase bridges. The EMBO journal *26*, 3397-3409.
511 Chan, K.L., Palmai-Pallag, T., Ying, S., and Hickson, I.D. (2009). Replication stress induces sister-
512 chromatid bridging at fragile site loci in mitosis. Nature cell biology *11*, 753-760.
513 Cloud, V., Chan, Y.L., Grubb, J., Budke, B., and Bishop, D.K. (2012). Rad51 is an accessory factor for
514 Dmc1-mediated joint molecule formation during meiosis. Science *337*, 1222-1225.
515 Costes, A., and Lambert, S.A.E. (2013). Homologous Recombination as a Replication Fork Escort: Fork-
516 Protection and Recovery. Biomolecules *3*, 39-71.
517 Cotta-Ramusino, C., Fachinetti, D., Lucca, C., Doksani, Y., Lopes, M., Sogo, J., and Foiani, M. (2005).
518 Exo1 processes stalled replication forks and counteracts fork reversal in checkpoint-defective cells.
519 Molecular cell *17*, 153-159.
520 Debatisse, M., Le Tallec, B., Letessier, A., Dutrillaux, B., and Brison, O. (2012). Common fragile sites:
521 mechanisms of instability revisited. Trends in genetics : TIG *28*, 22-32.
522 Dewar, J.M., Budzowska, M., and Walter, J.C. (2015). The mechanism of DNA replication termination
523 in vertebrates. Nature *525*, 345-350.
524 Dubarry, M., Loiodice, I., Chen, C.L., Thermes, C., and Taddei, A. (2011). Tight protein-DNA
525 interactions favor gene silencing. Genes & development *25*, 1365-1370.
526 Ge, X.Q., Jackson, D.A., and Blow, J.J. (2007). Dormant origins licensed by excess Mcm2-7 are
527 required for human cells to survive replicative stress. Genes & development *21*, 3331-3341.
528 Germann, S.M., Schramke, V., Pedersen, R.T., Gallina, I., Eckert-Boulet, N., Oestergaard, V.H., and
529 Lisby, M. (2014). TopBP1/Dpb11 binds DNA anaphase bridges to prevent genome instability. The
530 Journal of cell biology *204*, 45-59.
531 Glover, T.W., Berger, C., Coyle, J., and Echo, B. (1984). DNA polymerase alpha inhibition by
532 aphidicolin induces gaps and breaks at common fragile sites in human chromosomes. Human
533 genetics *67*, 136-142.
534 Granot, D., and Snyder, M. (1991). Segregation of the nucleolus during mitosis in budding and fission
535 yeast. Cell motility and the cytoskeleton *20*, 47-54.
536 Hashimoto, Y., Puddu, F., and Costanzo, V. (2011). RAD51- and MRE11-dependent reassembly of
537 uncoupled CMG helicase complex at collapsed replication forks. Nature structural & molecular
538 biology *19*, 17-24.
539 Hashimoto, Y., Ray Chaudhuri, A., Lopes, M., and Costanzo, V. (2010). Rad51 protects nascent DNA
540 from Mre11-dependent degradation and promotes continuous DNA synthesis. Nature structural &
541 molecular biology *17*, 1305-1311.
542 Helmrich, A., Ballarino, M., and Tora, L. (2011). Collisions between replication and transcription
543 complexes cause common fragile site instability at the longest human genes. Molecular cell *44*, 966-
544 977.
545 Higgs, M.R., Reynolds, J.J., Winczura, A., Blackford, A.N., Borel, V., Miller, E.S., Zlatanou, A.,
546 Nieminuszczy, J., Ryan, E.L., Davies, N.J.*, et al.* (2015). BOD1L Is Required to Suppress Deleterious
547 Resection of Stressed Replication Forks. Molecular cell *59*, 462-477.

548 Iraqui, I., Chekkal, Y., Jmari, N., Pietrobon, V., Freon, K., Costes, A., and Lambert, S.A. (2012).
549 Recovery of arrested replication forks by homologous recombination is error-prone. PLoS genetics *8*,
550 e1002976.
551 Jacome, A., and Fernandez-Capetillo, O. (2011). Lac operator repeats generate a traceable fragile site
552 in mammalian cells. EMBO reports *12*, 1032-1038.
553 Kawabata, T., Luebben, S.W., Yamaguchi, S., Ilves, I., Matise, I., Buske, T., Botchan, M.R., and Shima,
554 N. (2011). Stalled fork rescue via dormant replication origins in unchallenged S phase promotes
555 proper chromosome segregation and tumor suppression. Molecular cell *41*, 543-553.
556 Lambert, S., and Carr, A.M. (2013). Impediments to replication fork movement: stabilisation,
557 reactivation and genome instability. Chromosoma *122*, 33-45.
558 Lambert, S., Mizuno, K., Blaisonneau, J., Martineau, S., Chanet, R., Freon, K., Murray, J.M., Carr, A.M.,
559 and Baldacci, G. (2010). Homologous recombination restarts blocked replication forks at the expense
560 of genome rearrangements by template exchange. Molecular cell *39*, 346-359.
561 Lambert, S., Watson, A., Sheedy, D.M., Martin, B., and Carr, A.M. (2005). Gross chromosomal
562 rearrangements and elevated recombination at an inducible site-specific replication fork barrier. Cell
563 *121*, 689-702.
564 Laulier, C., Cheng, A., and Stark, J.M. (2011). The relative efficiency of homology-directed repair has
565 distinct effects on proper anaphase chromosome separation. Nucleic acids research *39*, 5935-5944.
566 Le Tallec, B., Dutrillaux, B., Lachages, A.M., Millot, G.A., Brison, O., and Debatisse, M. (2011).
567 Molecular profiling of common fragile sites in human fibroblasts. Nature structural & molecular
568 biology *18*, 1421-1423.
569 Le Tallec, B., Millot, G.A., Blin, M.E., Brison, O., Dutrillaux, B., and Debatisse, M. (2013). Common
570 fragile site profiling in epithelial and erythroid cells reveals that most recurrent cancer deletions lie in
571 fragile sites hosting large genes. Cell reports *4*, 420-428.
572 Lea, D.E., and Coulson, C.A. (1949). The distribution of the numbers of mutants in bacterial
573 populations. Journal of genetics *49*, 264-285.
574 Letessier, A., Millot, G.A., Koundrioukoff, S., Lachages, A.M., Vogt, N., Hansen, R.S., Malfoy, B., Brison,
575 O., and Debatisse, M. (2011). Cell-type-specific replication initiation programs set fragility of the
576 FRA3B fragile site. Nature *470*, 120-123.
577 Magdalou, I., Lopez, B.S., Pasero, P., and Lambert, S.A. (2014). The causes of replication stress and
578 their consequences on genome stability and cell fate. Seminars in cell & developmental biology *30*,
579 154-164.
580 Mankouri, H.W., Huttner, D., and Hickson, I.D. (2013). How unfinished business from S-phase affects
581 mitosis and beyond. The EMBO journal *32*, 2661-2671.
582 Miyabe, I., Mizuno, K., Keszthelyi, A., Daigaku, Y., Skouteri, M., Mohebi, S., Kunkel, T.A., Murray, J.M.,
583 and Carr, A.M. (2015). Polymerase delta replicates both strands after homologous recombination-
584 dependent fork restart. Nature structural & molecular biology *22*, 932-938.
585 Mizuno, K., Lambert, S., Baldacci, G., Murray, J.M., and Carr, A.M. (2009). Nearby inverted repeats
586 fuse to generate acentric and dicentric palindromic chromosomes by a replication template exchange
587 mechanism. Genes & development *23*, 2876-2886.
588 Mizuno, K., Miyabe, I., Schalbetter, S.A., Carr, A.M., and Murray, J.M. (2013). Recombination-
589 restarted replication makes inverted chromosome fusions at inverted repeats. Nature *493*, 246-249.
590 Moreno, S., Klar, A., and Nurse, P. (1991). Molecular genetic analysis of fission yeast
591 Schizosaccharomyces pombe. Methods in enzymology *194*, 795-823.
592 Naim, V., and Rosselli, F. (2009). The FANC pathway and BLM collaborate during mitosis to prevent
593 micro-nucleation and chromosome abnormalities. Nature cell biology *11*, 761-768.
594 Nguyen, M.O., Jalan, M., Morrow, C.A., Osman, F., and Whitby, M.C. (2015). Recombination occurs
595 within minutes of replication blockage by RTS1 producing restarted forks that are prone to collapse.
596 eLife *4*, e04539.
597 Ozeri-Galai, E., Lebofsky, R., Rahat, A., Bester, A.C., Bensimon, A., and Kerem, B. (2011). Failure of
598 origin activation in response to fork stalling leads to chromosomal instability at fragile sites.
599 Molecular cell *43*, 122-131.

600 Petermann, E., Orta, M.L., Issaeva, N., Schultz, N., and Helleday, T. (2010). Hydroxyurea-stalled
601 replication forks become progressively inactivated and require two different RAD51-mediated
602 pathways for restart and repair. Molecular cell *37*, 492-502.
603 Pietrobon, V., Freon, K., Hardy, J., Costes, A., Iraqui, I., Ochsenbein, F., and Lambert, S.A. (2014). The
604 chromatin assembly factor 1 promotes Rad51-dependent template switches at replication forks by
605 counteracting D-loop disassembly by the RecQ-type helicase Rqh1. PLoS biology *12*, e1001968.
606 Sabatinos, S.A., Ranatunga, N.S., Yuan, J.P., Green, M.D., and Forsburg, S.L. (2015). Replication stress
607 in early S phase generates apparent micronuclei and chromosome rearrangement in fission yeast.
608 Molecular biology of the cell *26*, 3439-3450.
609 Schlacher, K., Christ, N., Siaud, N., Egashira, A., Wu, H., and Jasin, M. (2011). Double-strand break
610 repair-independent role for BRCA2 in blocking stalled replication fork degradation by MRE11. Cell
611 *145*, 529-542.
612 Schlacher, K., Wu, H., and Jasin, M. (2012). A distinct replication fork protection pathway connects
613 Fanconi anemia tumor suppressors to RAD51-BRCA1/2. Cancer cell *22*, 106-116.
614 Schwartz, M., Zlotorynski, E., Goldberg, M., Ozeri, E., Rahat, A., le Sage, C., Chen, B.P., Chen, D.J.,
615 Agami, R., and Kerem, B. (2005). Homologous recombination and nonhomologous end-joining repair
616 pathways regulate fragile site stability. Genes & development *19*, 2715-2726.
617 Sofueva, S., Osman, F., Lorenz, A., Steinacher, R., Castagnetti, S., Ledesma, J., and Whitby, M.C.
618 (2011). Ultrafine anaphase bridges, broken DNA and illegitimate recombination induced by a
619 replication fork barrier. Nucleic acids research *39*, 6568-6584.
620 Terenna, C.R., Makushok, T., Velve-Casquillas, G., Baigl, D., Chen, Y., Bornens, M., Paoletti, A., Piel,
621 M., and Tran, P.T. (2008). Physical mechanisms redirecting cell polarity and cell shape in fission yeast.
622 Current biology : CB *18*, 1748-1753.
623 Tsang, E., Miyabe, I., Iraqui, I., Zheng, J., Lambert, S.A., and Carr, A.M. (2014). The extent of error-
624 prone replication restart by homologous recombination is controlled by Exo1 and checkpoint
625 proteins. Journal of cell science *127*, 2983-2994.
626 Velve-Casquillas, G., Costa, J., Carlier-Grynkorn, F., Mayeux, A., and Tran, P.T. (2010). A fast
627 microfluidic temperature control device for studying microtubule dynamics in fission yeast. Methods
628 in cell biology *97*, 185-201.
629 Watson, A.T., Garcia, V., Bone, N., Carr, A.M., and Armstrong, J. (2008). Gene tagging and gene
630 replacement using recombinase-mediated cassette exchange in Schizosaccharomyces pombe. Gene
631 *407*, 63-74.
632 Wilhelm, T., Magdalou, I., Barascu, A., Techer, H., Debatisse, M., and Lopez, B.S. (2014). Spontaneous
633 slow replication fork progression elicits mitosis alterations in homologous recombination-deficient
634 mammalian cells. Proceedings of the National Academy of Sciences of the United States of America
635 *111*, 763-768.
636 Win, T.Z., Mankouri, H.W., Hickson, I.D., and Wang, S.W. (2005). A role for the fission yeast Rqh1
637 helicase in chromosome segregation. Journal of cell science *118*, 5777-5784.
638 Woodward, A.M., Gohler, T., Luciani, M.G., Oehlmann, M., Ge, X., Gartner, A., Jackson, D.A., and
639 Blow, J.J. (2006). Excess Mcm2-7 license dormant origins of replication that can be used under
640 conditions of replicative stress. The Journal of cell biology *173*, 673-683.
641 Zellweger, R., Dalcher, D., Mutreja, K., Berti, M., Schmid, J.A., Herrador, R., Vindigni, A., and Lopes, M.
642 (2015). Rad51-mediated replication fork reversal is a global response to genotoxic treatments in
643 human cells. The Journal of cell biology *208*, 563-579.
644 Zierhut, C., and Diffley, J.F. (2008). Break dosage, cell cycle stage and DNA replication influence DNA
645 double strand break response. The EMBO journal *27*, 1875-1885.

646

647

648

649 **Figure Legends**

650 **Figure 1: A single terminal fork arrest requires Rad52 for rescue by the opposite fork**

651 **A.** Diagram of the *t-LacO-ura4<ori* construct containing a single *RTS1*-RFB (< and blue bars) blocking
652 the progression of replication forks moving in the main replication direction, from the centromere
653 towards the telomere. Main replication origins (ori, black circles) located upstream and downstream
654 from the *RTS1*-RFB are indicated. GFP-LacI (green ellipses) bound to *LacO* arrays (green bars) are
655 integrated ~7 kb away from the *RTS1*-RFB, on the telomere-proximal side of *ura4* gene (red bar).
656 When Rtf1 is expressed, >90% of forks emanating from the strong centromere-proximal replication
657 origin, and moving towards the telomere, are blocked. In the absence of homologous recombination,
658 forks blocked at the *RTS1*-RFB are irreversibly-arrested. The replication of *LacO* arrays, either through
659 the progression of forks restarted by homologous recombination or by opposite forks, results in
660 sister LacI-foci in G2 cells. A failure of opposite forks to progress would result in a lower frequency of
661 sister LacI-foci. See Extended Data Fig.1 for more details.
662 **B.** Quantification and representative examples of mitotic abnormalities (indicated by a white arrow).
663 Values are means of at least three independent experiments ± the standard error of the mean (SEM).
664 Statistical analysis was performed with Mann-Whitney U tests.
665 **C.** Example of cells showing a single LacI-focus (green arrow) and sister LacI-foci (red arrow).
666 **D.** Quantification of cells with sister LacI-foci in G2. Values are means of at least three independent
667 experiments ± SEM. No statistical differences were observed between *wt* and *rad52-d* cells upon
668 induction of the *RTS1*-RFB, indicating a similar efficiency and timing of *LacO* arrays replication. These
669 data demonstrate that replication forks traveling from the telomere-proximal side of the *RTS1*-RFB
670 towards the centromere are not altered in the absence of homologous recombination.
671 Strains used: *wt*= AA23, *rad52-d*= AA1.
672

673 **Figure 2: Upon activation of the *RTS1*-RFB, anaphase bridges containing terminal polar fork arrests**
674 **break during progression through mitosis**

675 **A.** Temporal kinetics of mitotic bridge formation and resolution in the first 30 minutes after early
676 anaphase, from time-lapse movies.
677 **B.** Tracking of individual *LacO*-bridges during mitotic progression and cytokinesis from time-lapse
678 movies.
679 **C.** Example of anaphase bridges (white arrow) breaking during cytokinesis. See Extended Data Fig.2
680 for additional examples.
681 Strains used: *wt*= AA23, *rad52-d*= AA1.
682

683 **Figure 3: Rad52 restricts Exo1-mediated resection of unbroken forks**

684 **A.** Diagram of the *t-ura4<ori* construct containing a single *RTS1*-RFB. See Figure 1 for details.
685 **B.** Analysis of RPA recruitment to the active *RTS1*-RFB, based on chromatin immunoprecipitation
686 (ChIP). The fold-enrichment in RPA in the ON condition (RFB active) relative to the OFF condition (RFB
687 inactive) is shown. Upstream and downstream distances from the RFB are indicated in kilobases (kb).
688 Values are means of at least three independent experiments ± SEM. Statistical analysis was
689 performed using Mann-Whitney U tests. Strains used: *wt*=YC219, *rad52-d*=YC223, *exo1-d*=YC221,
690 *rad52-d exo1-d*=AC434.
691 **C.** Analysis of ssDNA levels upstream from the active *RTS1*-RFB, by qPCR. The data shown are the
692 fold-enrichment in ssDNA in ON condition (RFB active) relative to OFF condition (RFB inactive).
693 Distances upstream from the RFB are indicated in base pairs (bp). A locus located on chromosome II
694 is used as a control. Values are means of at least three independent experiments ± SEM. Statistical
695 analysis was performed with Mann-Whitney U tests. Strains used: *wt*=YC13, *rad52-d*=YC90, *exo1-*
696 *d*=II258, *rad52-d exo1-d*=AA15.
697 **D.** Scheme of replication intermediates (RIs) observed in a neutral-neutral 2DGE analysis of the *Ase*I
698 restriction fragment upon activation of the *RTS1*-RFB. See Extended Data Fig.3A-B for neutral-alkaline
699 2DGE analysis demonstrating that the tail signal contains newly replicated strands undergoing Exo1-
700 mediated degradation.
701 **E.** Representative RI analysis by 2DGE in the absence (RFB OFF) or presence of fork blockade (RFB
702 ON). A DNA fragment corresponding to *ura4* gene was used as probe. Numbers indicate the
703 efficiency of the RFB for each strain analyzed; values are means of at least three independent
704 experiments ± standard deviation (SD). Strains used: *wt*=YC13, *rad52-d*=YC90, *exo1-d*=II258, *rad52-d*
705 *exo1-d*=AA15. See Extended Data Fig. 3C for the *rad52-d rad50-d* double mutant.
706 **F.** Quantification of % of fork undergoing resection (tail signals) relative to the number of blocked
707 forks. Values are means of at least three independent experiments ± the 99% confidence interval
708 (99% CI).
709

710 **Figure 4: Anaphase bridges are RPA-positive and unresolved intertwined sister chromatids at the**
711 **site of terminal fork arrest**

712 **A.** Representative images showing RPA foci (labeled with Ssb3-mcherry) merging/touching GFP-LacI
713 foci cells harboring the *t-LacO-ura4<ori* construct shown in Fig. 1A. Of note, *rad52-d* strains have a
714 number of cells with multiple RPA foci. To avoid biases toward a random localization of GFP-LacI and
715 RPA foci, cells with ≥ 3 RPA foci were excluded from the analysis. See Extended Data Fig.4 for
716 additional examples.

717 **B.** Quantification of cells showing RPA recruited to the *RTS1*-RFB, according to cell cycle phase. G2
718 and S-phase cells are mononucleated cells and binucleated cells with a septum, respectively. Values
719 are means of at least three independent experiments ± SEM. Statistical analysis was performed with
720 Mann-Whitney U tests.
721 **C.** Representative example of mitotic RPA-positive *LacO*-bridges (left panel) and their quantification
722 (right panel).
723 **D.** Example of a mitotic RPA-positive *LacO*-bridge emanating from an early anaphase in which a single
724 RPA focus is located at the nexus of the two nuclei, in a *rad52-d* cell. See Extended Data Fig.4 for
725 additional examples.
726 **E.** Classification and quantification of mitotic *LacO*-bridges in *rad52-d* cells, according to their origin,
727 from time-lapse movies. $RPA^+/LacI^+$ and $RPA^+/LacI^-$ denote an RPA focus touching/merging, or not, a
728 GFP-LacI focus, respectively.
729 **F.** Schematic interpretation of *LacO*-bridges at unprotected forks.
730 Strains used: *wt*=AS39, *rad52-d*=SL1190, *exo1-d*=AA46, *rad52-d exo1-d*=SL1194.
731

732 **Figure 5: Excess RPA-coated ssDNA gaps at terminal fork arrest causes a failure of mitotic sister**
733 **chromatid disjunction and genome instability**

734 **A.** Quantification of mitotic defects. Values are means of at least three independent experiments ±
735 SEM. Statistical analysis was performed with Mann-Whitney U tests. Strains used: *rad52-d*=AA1,
736 *exo1-d*=AA39, *rad52-d exo1-d*=AA42. See Extended Data Fig. 3 for mitotic index and cell cycle
737 distribution.
738 **B.** Diagram of the *t<ura4-ori* construct. A loss of *ura4* function was selected on 5-fluoroorotic acid (5-
739 FOA)-containing plates, following several generations, with or without induction of the *RTF1*-RFB.
740 **C.** Rate of *ura4* loss (number of 5FOA-resistant colonies/cell/division). Values are the median rate ±
741 95 CI. Statistical analysis was performed with the Mann-Whitney U test. Strains used: *wt*=SL504,
742 *rad52-d*=AA95, *exo1-d*=AA91, *rad52-d exo1-d*=AA98.
743 **D.** Cell survival after spreading onto minimal medium without thiamine (RFB ON), expressed relative
744 to the survival of the same strains spread onto minimal medium containing thiamine (RFB OFF).
745 Values are means of at least three independent experiments ± the 95% CI. Strains used: *wt*=YC266,
746 *rad52-d*=YC270, *exo1-d*=II558, *rad52-d exo1-d*= YC274.
747

748 **Figure 6: Rad51 binding to DNA is sufficient to ensure the rescue of terminal fork arrest by opposite**
749 **forks**

750 **A**. Tenfold serial dilution of indicated strains on plates containing indicated doses of bleomycin and
751 MMS. See Extended Data Fig.5 for the characterization of the *rad51-3A* mutant. Strains used:
752 *wt*=AA109, *rad51-3A*=AA118, *rad51-d*=SL1010.
753 **B.** Diagram of the *t-ura4-sd20<ori* construct containing a single *RTS1*-RFB. The non-functional *ura4-*
754 *sd20* allele harbors a 20-nucleotide duplication flanked by micro-homology. Cells are thus auxotroph
755 for uracil. HR-mediated fork restart is associated to a non-processive DNA synthesis, liable to
756 replication slippage at micro-homology. When forks are restarted at the *RTS1*-RFB, the *ura4-sd20*
757 gene is replicated by a restarted fork which the non-processive DNA synthesis undergoes replication
758 slippage. This results in the deletion of the duplication and the restoration of a functional *ura4*$^{+}$ gene.
759 **C.** Frequency of replication slippage. "No RFB" indicates conditions in which strains harbor the *t-*
760 *ura4-sd20-ori* construct without the *RTS1*-RFB. Values are means of at least three independent
761 experiments ± the 95% CI. Strains used: *wt* noRFB=AA124, *wt* RFB ON=AA129, *rad51-d* no RFB=YC76,
762 *rad51-d* RFB ON=YC80, *rad51-3A* no RFB=AA139, *rad51-3A* RFB ON=AA133.
763 **D.** Representative RI analysis by 2DGE, in the absence (RFB OFF) or presence (RFB ON) of fork
764 blockade. A DNA fragment corresponding to *ura4* gene was used as probe. The numbers indicate the
765 efficiency of the *RTS1*-RFB for each strain analyzed; values shown are means of at least three
766 independent experiments ± SD. The bottom histogram shows % of fork undergoing resection (tail
767 signals) relative to the number of blocked forks. Values are means of at least three independent
768 experiments ± the 99% CI. Strains used: *wt*=AA129, *rad51-d*=YC80, *rad51-3A*=AA133.
769 **E.** Quantification of mitotic defects. Values are means of at least three independent experiments ±
770 SEM. Statistical analysis was performed with the Mann-Whitney U test. Strain used: *wt*=AA23, *rad51-*
771 *d*=AC409, *rad51-3A*=AA158.
772
773 **Figure 7: Model of unprotected fork-induced anaphase bridges**
774 Rad51-dependent fork restart and protection are genetically separable.
775
776
777
778
779
780
781
782
783
784

785 **STAR Methods**

786

787 **KEY RESOURCES TABLE**

788

789 **CONTACT FOR REAGENT AND RESOURCE SHARING**

790 Further information and requests for resources and reagents should be directed to and will be
791 fulfilled by the Lead Contact, Dr Sarah AE Lambert (sarah.lambert@curie.fr)

792

793 **EXPERIMENTAL MODEL AND SUBJECT DETAILS**

794 Yeast strains were freshly thawed from frozen stocks and grown at 30°C using standard yeast
795 genetics practices.

796

797 **METHOD DETAILS**

798 ***Standard yeast genetics***

799 The yeast strains used in this work are listed in supplemental Table 1. Gene deletion and tagging
800 were performed with classical and molecular genetics techniques (Moreno et al., 1991). Strains
801 carrying the replication fork barrier *RTS1* were grown in supplemented EMM-glutamate. The *RTS1*
802 barrier was kept inactive by adding 60 µM thiamine to the media (RFB OFF conditions). The *RTS1*
803 barrier was activated by transfer into thiamine-free medium and incubation for 24 hours, in most
804 experiments. The *rad51-3A* mutant was obtained by recombinase-mediated cassette exchange, as
805 previously described (Watson et al., 2008). For cell sensitivity to genotoxic drugs, MMS (Sigma,
806 129925) and Bleomycin (Bellon, 525709) were added to the media on plates.

807 ***Analysis of replication intermediates by 2DGE***

808 Replication intermediates (RIs) were analyzed by 2DGE, as follows: $2.5x10^9$ cells were washed in
809 water, resuspended in 20 ml of cold water and transferred to a glass/Pyrex Petri dish on ice. Genomic
810 DNA was crosslinked with trimethyl psoralen (TMP, Sigma, T6137) as follows: cell suspensions were
811 mixed with 1 ml TMP (0.2 mg/ml in ethanol) and incubated in the dark for 5 minutes, with occasional
812 swirling. Cells were exposed to UVA (365 nm) for 90 seconds, at a flow rate of 50 mW/cm². Cells
813 were treated with 0.625 mg/ml lysing enzyme (Sigma, L1412) and 0.5 mg/ml zymolyase 100T
814 (Amsbio, 120493-1). The resulting spheroplasts were then embedded in low-melting point agarose
815 (InCert Agarose, Lonza) plugs, incubated in a digestion buffer containing proteinase K (Euromedex,
816 EU0090) and stored in TE (50 mM Tris, 10 mM EDTA). DNA was digested with 60 units per plug of the
817 restriction enzyme *Ase*I (NEB, R0526M) and then treated with RNase (Roche, 11119915001) and
818 beta-agarase (NEB, M0392L). Melted Plugs were equilibrated with 0.3M NaCl and RI enrichment was

819 achieved on BND cellulose (Sigma, B6385) embedded in columns (Biorad, 731-1550), as described
820 (Lambert et al., 2010). RIS were enriched in the 1M NaCl 1.8% caffeine (Sigma, C-8960). After
821 precipitation with glycogen (Roche, 10901393001), RIs were separated by electrophoresis in 0.35%
822 and 0.9% (+ EtBr) agarose gels in 1X TBE for the first and second dimensions (Brewer et al., 1992). For
823 2DGE in denaturing conditions, the second dimension involved migration in alkaline buffer (5 mM
824 NaOH, 1 mM EDTA). DNA was transferred to a nylon membrane (Perkin Elmer, NEF988001PK) in 10X
825 SSC and probed with a ^{32}P-radiolabeled *ura4* sequence (GE healthcare rediprime II, RPN1633, and
826 alpha-32P dCTP, Perkin Elmer, BLU013Z250UC) in Ultra-Hyb buffer (Invitrogen, AM8669) at 42°C.
827 Quantitative densitometric analysis of the Southern-blots was carried out using ImageQuant
828 software (GE healthcare).

829 ***Live cell imaging***

830 Cells were prepared as previously described (Pietrobon et al., 2014). Cells were cultured in
831 glutamate-supplemented EMM, with or without thiamine, washed twice and resuspended in fresh
832 filtered medium. A 1-2 µl drop of exponentially growing culture was deposited on the well of a
833 microscope slide (Thermo Scientific, ER-201B-CE24) covered with 1.4% agarose in filtered EMM.
834 Images were acquired with a 3D microscope (LEICA DMRXA) equipped with a CoolSNAP
835 monochromic camera (Roper Scientific). Cells were visualized with a 100X oil immersion objective
836 with a numerical aperture of 1.4 and Z-stack images were captured with METAMORPH software.
837 Image acquisition and analysis were performed on the workstations of the PICT-IBiSA Orsay Imaging
838 facility of Institut Curie.

839 For time-lapse movies, cells were injected into dedicated 4-5 µm-thick poly-dimethyl-siloxane
840 (PDMS) microfluidic chambers on glass coverslips, as previously described (Terenna et al., 2008)
841 (Velve-Casquillas et al., 2010). Images were acquired with a Nikon Eclipse Ti-E microscope equipped
842 with the perfect Focus System, a 100X/1.45-NA PlanApo oil immersion objective, a Mad City Lab
843 piezo stage, a Yokogawa CSUX1 confocal unit, a Photometrics HQ2 CCD camera and a laser bench
844 (Errol) with 491 and 561 nm diode lasers, 100mX each (Cobolt). Images were acquired every 5
845 minutes. For M-cherry and GFP fluorescence, images were acquired with an acquisition time of 300
846 ms at 12% power and 500 ms at 17% power. Movies were constructed with METAMORPH software
847 and analyzed with ImageJ software.

848 ***Analysis of ssDNA by qPCR***

849 $2x10^8$ cells were mechanically lysed by vortexing with glass beads (425-600 µm, Sigma®). Genomic
850 DNA was extracted by the classical phenol/chloroform method. We incubated 5 µg of DNA with or
851 without 100 units of the restriction enzyme *Mse*I (NEB, R0525M) which cuts dsDNA within the PCR

852 amplicon to discriminate between ds and ssDNA . We then subjected 30 ng of the digested or mock-
853 digested DNA to amplification by qPCR (iQ SYBR green supermix, Biorad, 1708882), using primers
854 annealing on either side of the *Mse*I restriction site (primers listed in table 2). We quantified ssDNA
855 as previously described (Zierhut and Diffley, 2008), using the formula: ssDNA $=100/((1+2^{\Delta Ct})/2)$, in
856 which ΔCt is the difference between the threshold cycles of digested and undigested DNA. A control
857 locus (II-150) with no *Mse*I restriction sites, for which the Ct values for digested and undigested DNA
858 would be expected to be similar, was used to correct the ΔCt values of other primers and to
859 normalize the results relative to the amount of DNA initially loaded onto the plate.

860 ***Chromatin immunoprecipitation of RPA***

861 RPA enrichment at *RTS1*-RFB was performed using strains expressing a tagged RPA subunit, Ssb3-YFP.
862 ChIP experiments were performed as previously described (Tsang et al., 2014). Samples were
863 crosslinked with 10 mM DMA (dimethyl adipimidate, thermos scientific, 20660) and 1%
864 formaldehyde (Sigma, F-8775). Chromatin was sonicated with a Diagenod Bioruptor set on high for
865 10 cycles of 30 seconds ON + 30 seconds OFF. Immunoprecipitation was performed with an anti-GFP
866 antibody (rabbit polyclonal, Molecular probe, A11122) at 1:300 and Protein G Dynabeads (Invitrogen,
867 10003D) for the detection of Ssb3-YFP. The DNA associated with RPA was purified with a Qiaquick
868 PCR purification kit (Qiagen, 28104) and eluted in 200 µl of water. The relative amount of DNA was
869 determined by qPCR (iQ SYBR green supermix, Biorad, 1708882, primers listed in Table 2). RPA
870 enrichment was normalized relative to an internal control locus (*ade6*). RPA enrichment in the ON
871 condition is shown relative to enrichment in the OFF condition.

872 ***Replication slippage assay***

873 Replication slippage was assessed with the *ura4-sd20* allele (initially named *ura4-dup20*), as
874 previously described (Iraqui et al., 2012). 5FOA (Euromedex, 1555)-resistant colonies were grown on
875 uracil-containing plates without thiamine for 2 days at 30°C, and were then used to inoculate uracil-
876 containing medium without thiamine, in which they were incubated for 24 h. Cells were
877 appropriately diluted and plated on YE plates (for survival counting) and uracil-free plates
878 supplemented with thiamine. After 5 days of incubation at 30°C, colonies were counted to determine
879 the frequency of replication slippage.

880 ***RFB-induced loss of ura4 function***

881 The loss of *ura4* marker was performed as previously described (Iraqui et al., 2012). Single $Ura4^+$
882 colonies were streaked on plates containing uracil, with or without thiamine. At least 11 independent
883 single colonies for each strain and condition were used to inoculate medium containing uracil, with
884 or without thiamine, and the culture was incubated until stationary phase was reached. Appropriate

885 dilutions were plated on supplemented YE plates (to determine cell survival) and YE plates containing
886 0.1% 5-FOA (Euromedex, 1555). Colonies were counted after 5-7 days of incubation at 30°C. The
887 rates of *ura4* loss were calculated as described in (Lea and Coulson, 1949). Each fluctuation test was
888 repeated two or three times. Statistical analysis was performed with the Mann-Whitney U test.

889 ***Cell viability***

890 Cells were grown on supplemented EMM without thiamine for 14 hours. They were then used to
891 prepare appropriate dilutions for plating on EMM plates with (RFB OFF) or without (RFB ON)
892 thiamine. Colonies were counted after 5-7 days of incubation at 30°C and viability was calculated as
893 the ratio of the number colonies growing in ON conditions relative to the number growing in OFF
894 conditions.

895 ***Rad51 foci detection by immunofluorescence***

896 Exponentially growing cells were treated or not with 0.3% MMS (Sigma 129925) for 1 hour. Cells
897 were fixed with 4% paraformaldehyde (Alfa Aesar 30525-89-4) in PEM (100mM PIPES, 1mM EGTA,
898 1mM MgSO4, pH 6.9) for 5 min at 30 °C, then washed in PBS and then with PEM. Cells were digested
899 in 1.25mg/ml Zymolyase 20T (amsbio 120491-1) in PEMS (1.2M sorbitol in PEM) at 37°C for 70
900 minutes. After washing 3 times in PEMS, cells were treated with 1% triton 100X in PEMS for 5 min at
901 room temperature. Cells were washed twice with PEMBAL (1% BSA, 0.1% sodium azide, 100mM
902 lysine monohydrate (Sigma L-5626) in PEM) and incubated for 1 hour on the wheel in PEMBAL. Cells
903 were resuspended in 300µl of PEMBAL containing anti-Rad51 (Thermo Scientific PA1-4968) at 1/500
904 and then incubated overnight on the wheel at room temperature. After several quick washes with
905 PEMBAL followed by one wash of 30 minutes, cells were resuspended in 300µl of PEMBAL containing
906 anti-Rabbit Alexa Fluor® 555 (Molecular Probes A21428) at 1/1000 for 4 hours at room temperature.
907 After several washes with PBS, cells were re-suspended in 1ml of PBS containing 100µM of sodium
908 azide. For microscopy, cells were spread on a regular slid, dried and then covered with a drop of
909 ProLong® Gold antifade reagent with DAPI (Molecular Probes P36935) before to place a cover slip.
910

911 **QUANTIFICATION AND STATISTICAL ANALYSIS**

912 Quantitative densitometric analysis of the Southern-blots (2DGE) was performed using ImageQuant
913 software. The "tail signal" was normalized to the total signal of arrested forks.
914 Cell images were collected using METAMORPH software and analyzed using ImageJ software.
915 The definitions of values and errors bars are mentioned in the figures legend. For most experiments,
916 the number of sample is n> 3 obtained from independent experiments to ensure biological
917 reproducibility. Statistical analysis was performed using using Mann-Whitney U tests and the student

t-test. When no statistics are mentioned, errors bars correspond to the 99 or 95 % confidence interval (Figure, 3F, 5B and 6D).

DATA AND SOFTWARE AVAILABILITY

Data have been deposited to Mendeley data and are available at
http://dx.doi.org/10.17632/j745gb53ys.1

KEY RESOURCES TABLE

REAGENT or RESOURCE	SOURCE	IDENTIFIER
Antibodies		
Anti-Rad51	Thermo-scientific	PA1-4968
Anti-PCNA	Santa Cruz	Pc10:Sc56
Anti-GFP	Molecular probe	A11122
Alexa fluor 555 goat anti-rabbit	Molecular probe	A21428
Bacterial and Virus Strains		
Biological Samples		
Chemicals, Peptides, and Recombinant Proteins		
Trioxsalen (Tri-methyl psoralen)	Sigma	T6137
Proteinase K	Euromedex	EU0090
RNase A DNase-free	Roche	11119915001
Incert agarose	Lonza	50123
Lysing enzymes	Sigma	L1412
Zymolyase 20T	Amsbio	120491-1
Zymolyase 100T	Amsbio	120493-1
Benzoylated Naphthoylated DEAE-cellulose (BND)	Sigma	B6385
Gene Screen Plus nylon membrane	Perkin Elmer	NEF988001PK
Dynabeads protein G	Invitrogen	10003D
Mse1	New England Biolabs	R0525M
CutSmart buffer	New England Biolabs	B7204S
Ase1 High concentration	New England Biolabs	R0526M
NEB Buffer 3.1	New England Biolabs	B7203S
Beta agarase	New England Biolabs	M0392L
Slide for microscopy 8 wells 6mm	Thermo Scientific	ER-201B-CE24
5-FOA	Euromedex	1555
Bleomycine	Bellon	525709
Methyl methane sulfonate MMS	sigma	129925
Ultra-Hyb buffer	Invitrogen	AM8669
DMA	Thermo Scientific	20660
Glycogen	Roche	10901393001
Caffeine	Sigma	C-8960
Poly-prep Chromatography columns	Biorad	731-1550
ProLong® Gold antifade reagent with DAPI	Molecular Probes	P36935
Lysine monohydrate	Sigma	L-5626
Paraformaldehyde	Alfa Aesar	30525-89-4
DEOXYCYTIDINE 5'-triphosphate [alpha-32P]	Perkin Elmer	BLU013Z250UC
Formaldehyde	Sigma	F-8775
Critical Commercial Assays		
Rediprime II	GE healthcare	RPN1633
iQ SYBR green supermix	Biorad	1708882
Qiaquick PCR purification	Qiagen	28104
Deposited Data		
Mendeley Data	*https://data.mendeley.com/*	http://dx.doi.org/10.17632/j745gb53ys.1

Experimental Models: Cell Lines		
Experimental Models: Organisms/Strains		
See Table S1 for a list of yeast strains used in this study	Lambert's lab	Strain number
Oligonucleotides		
See Table S2 for a list of oligonucleotides used in this study	Sigma	N/A
Recombinant DNA		
Software and Algorithms		
Image processing and analysis in Java	Image J	https://imagej.nih.gov/ij/
Image Quant TL	GE healtcare	http://gelifesciences.com
MetaMorph Microscopy Automation and Image Analysis Software	Molecular devices	https://www.moleculardevices.com
Other		

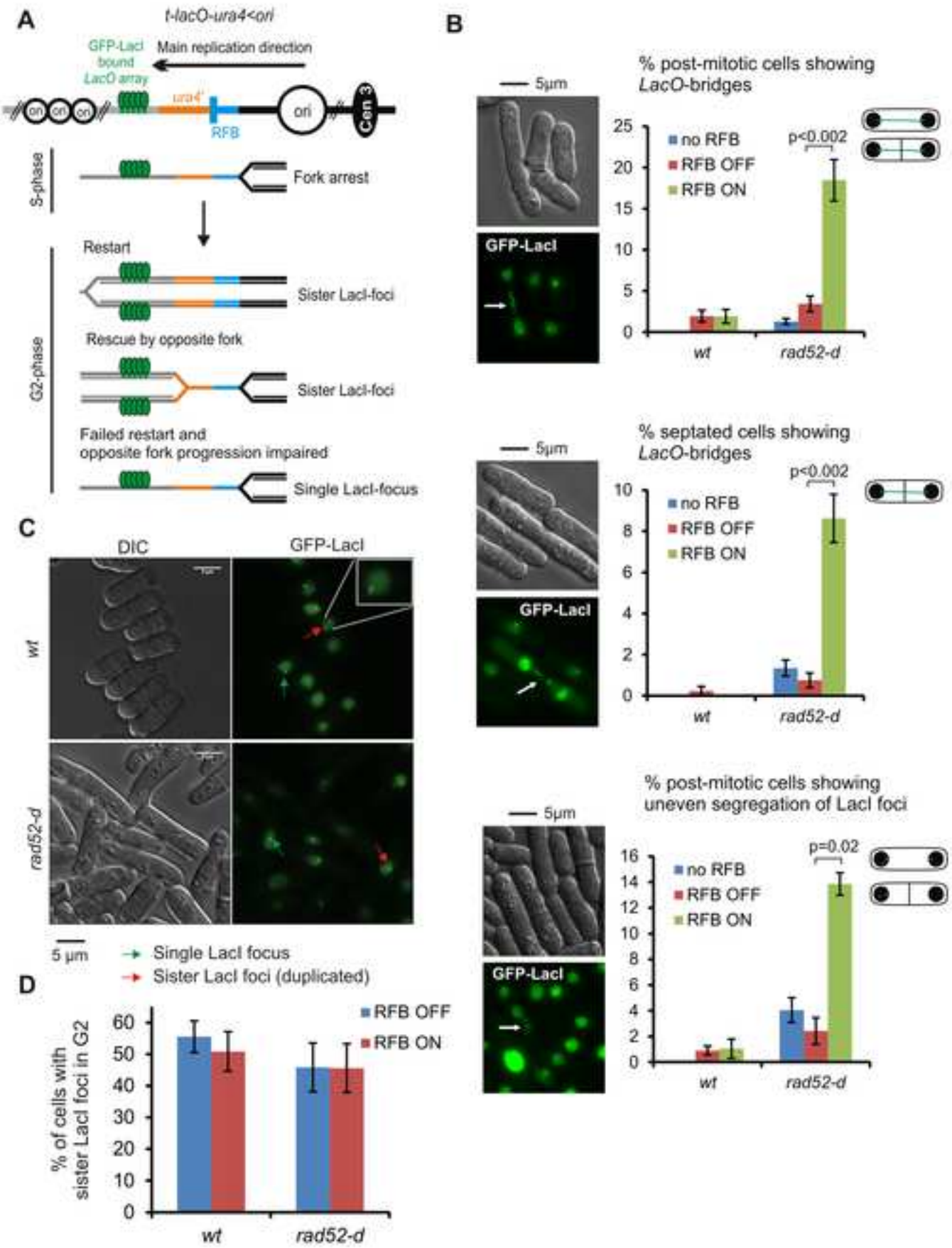
A
t-lacO-ura4<ori
GFP-LacI bound LacO array
Main replication direction
ori
ura4+
RFB
Cen 3
S-phase
Fork arrest
Restart
Sister LacI-foci
G2-phase
Rescue by opposite fork
Sister LacI-foci
Failed restart and opposite fork progression impaired
Single LacI-focus
B
% post-mitotic cells showing LacO-bridges
5µm
GFP-LacI
no RFB
RFB OFF
RFB ON
p<0.002
wt
rad52-d
% septated cells showing LacO-bridges
p<0.002
% post-mitotic cells showing uneven segregation of LacI foci
p=0.02
C
DIC
GFP-LacI
wt
rad52-d
5 µm
Single LacI focus
Sister LacI foci (duplicated)
D
% of cells with sister LacI foci in G2
RFB OFF
RFB ON
wt
rad52-d

Figure2

Click here to download Figure ait-saada et al Figure 2.tif

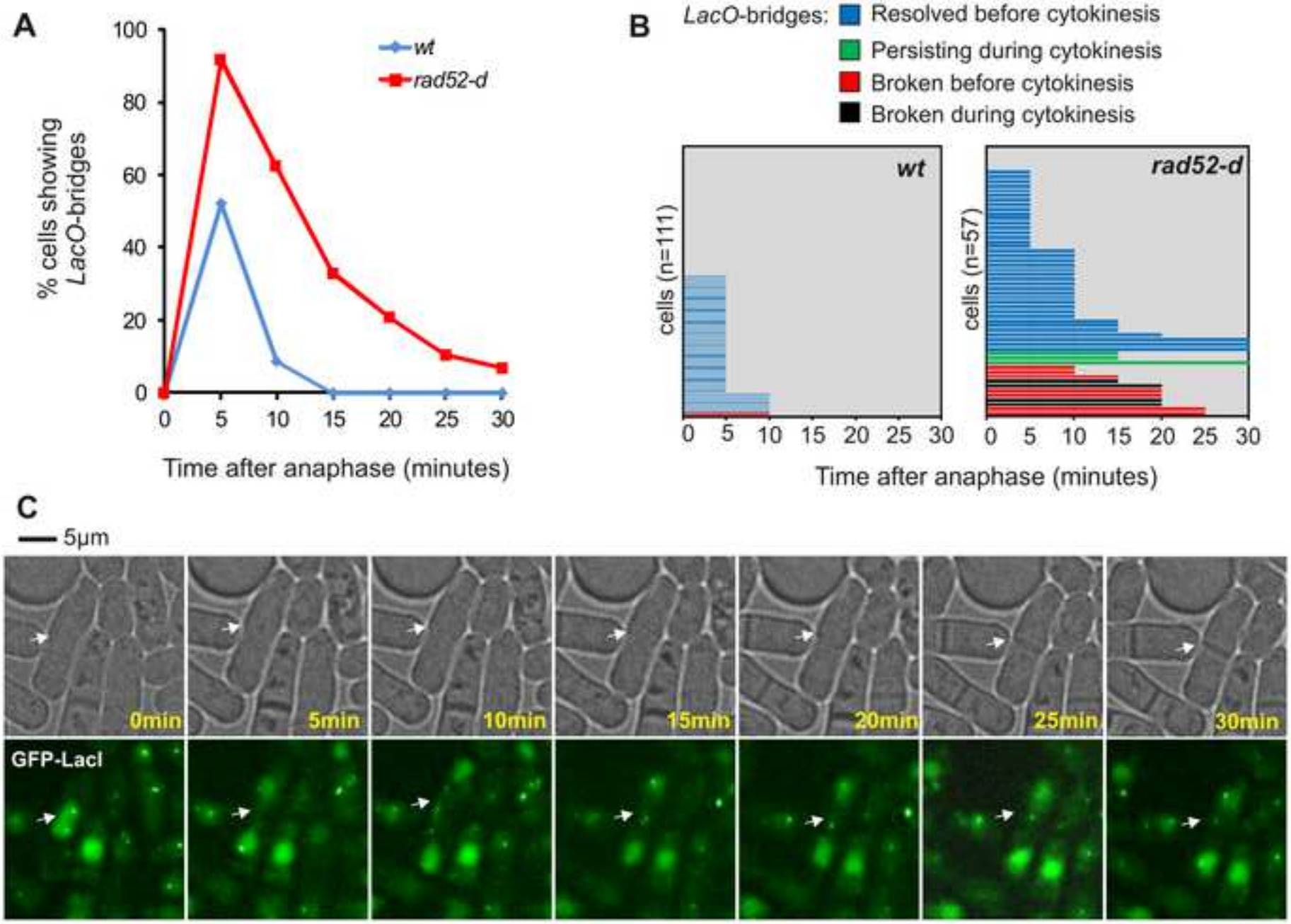

Figure3

Click here to download Figure ait-saada et al Figure 3.tif

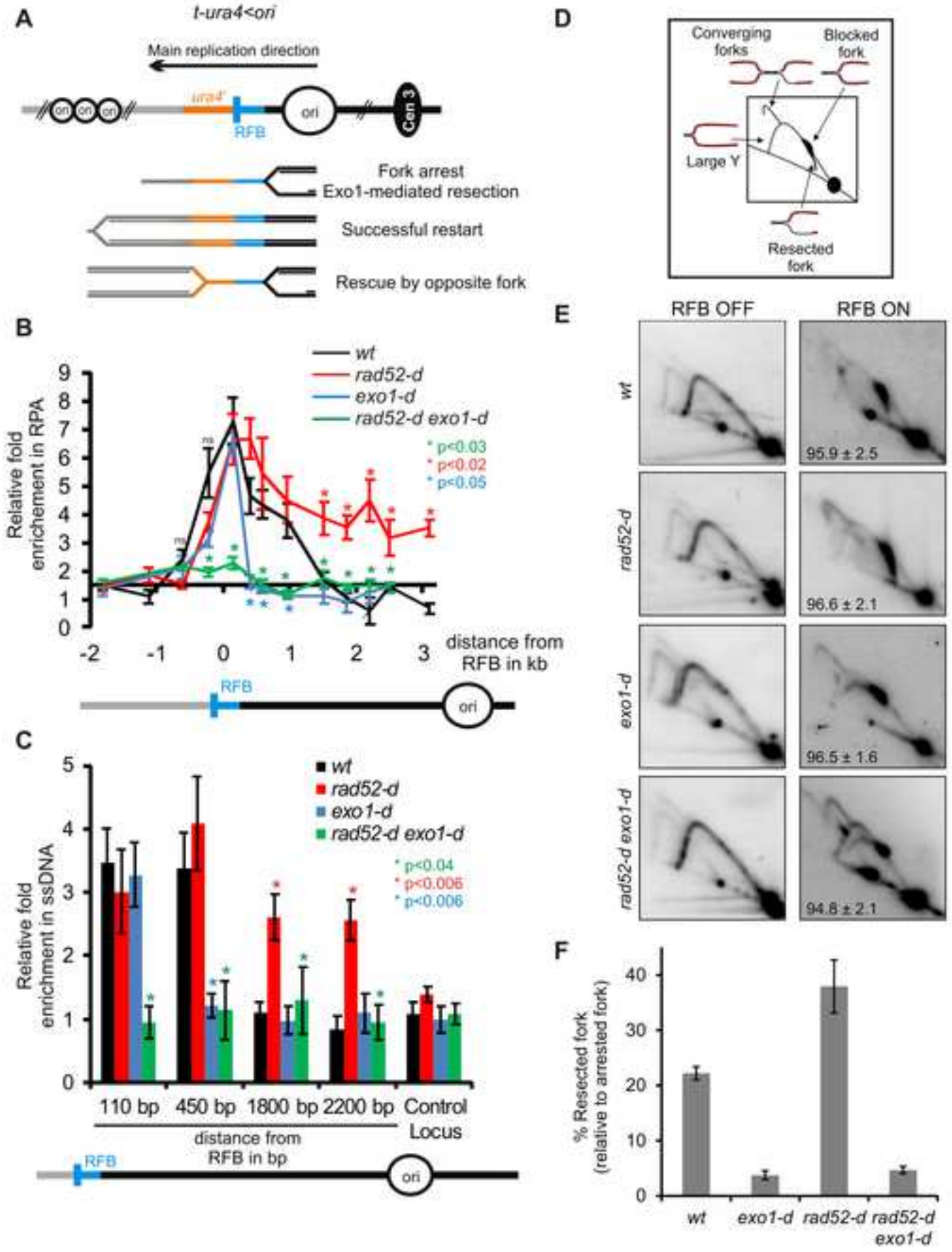

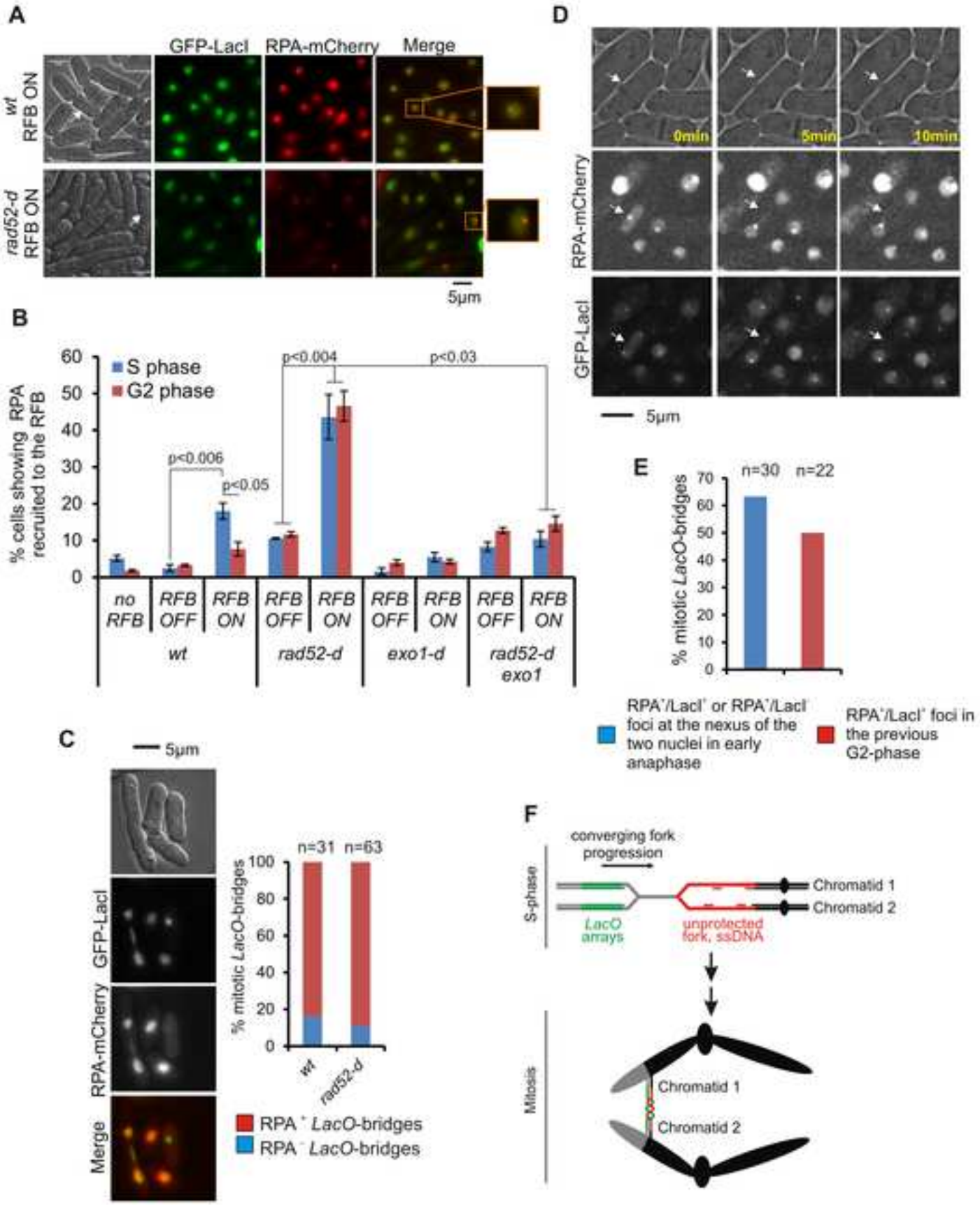
A
GFP-LacI
RPA-mCherry
Merge
wt RFB ON
rad52-d RFB ON
5µm
B
S phase
G2 phase
% cells showing RPA recruited to the RFB
p<0.006
p<0.05
p<0.004
p<0.03
no RFB
RFB OFF
RFB ON
wt
rad52-d
exo1-d
rad52-d exo1
C
5µm
GFP-LacI
RPA-mCherry
Merge
% mitotic LacO-bridges
n=31
n=63
wt
rad52-d
RPA+ LacO-bridges
RPA- LacO-bridges
D
0min
5min
10min
RPA-mCherry
GFP-LacI
5µm
E
% mitotic LacO-bridges
n=30
n=22
RPA+/LacI+ or RPA+/LacI- foci at the nexus of the two nuclei in early anaphase
RPA+/LacI+ foci in the previous G2-phase
F
converging fork progression
S-phase
Chromatid 1
Chromatid 2
LacO arrays
unprotected fork, ssDNA
Mitosis
Chromatid 1
Chromatid 2

Click here to download Figure ait-saada et al Figure 5.tif

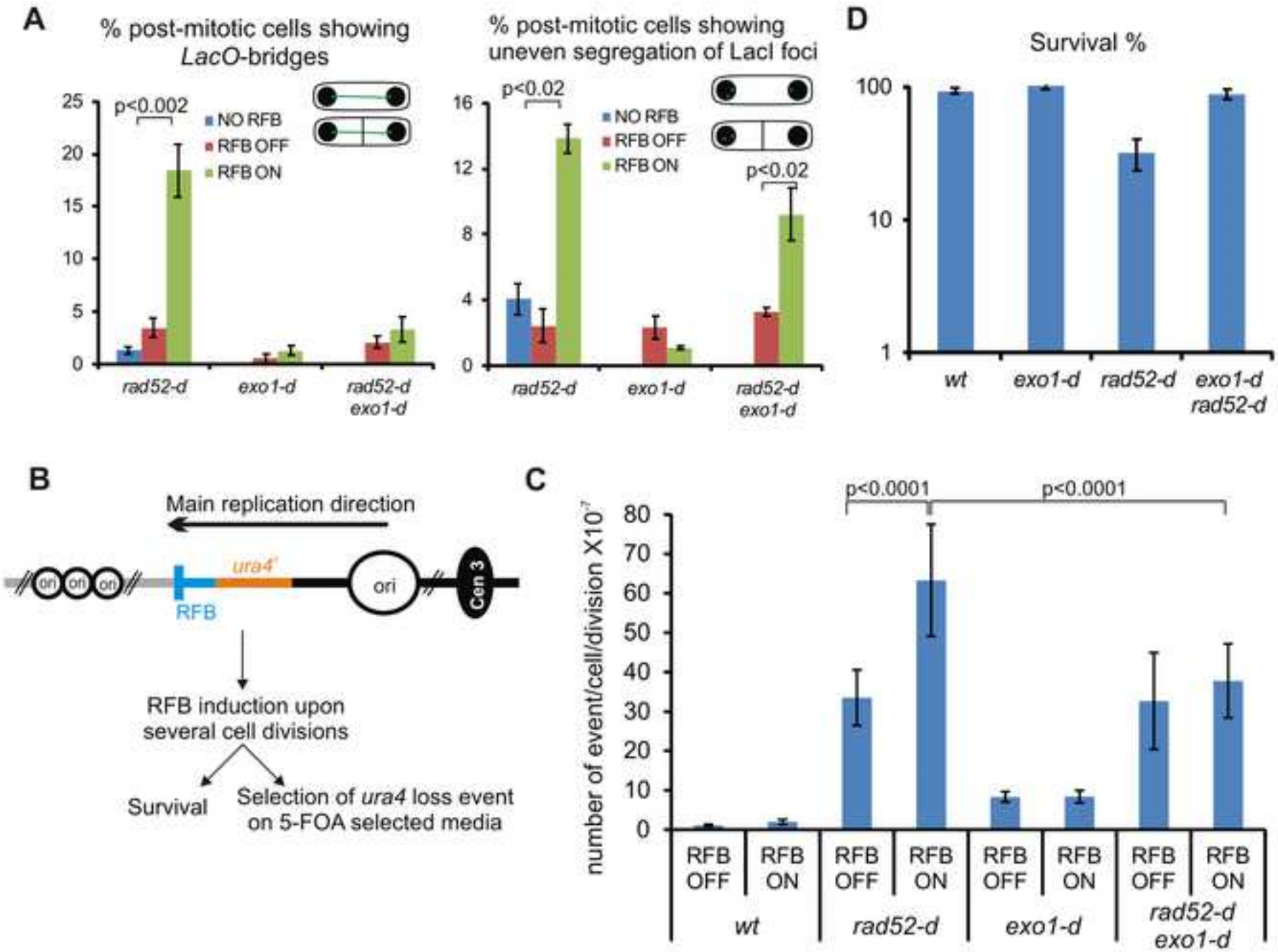

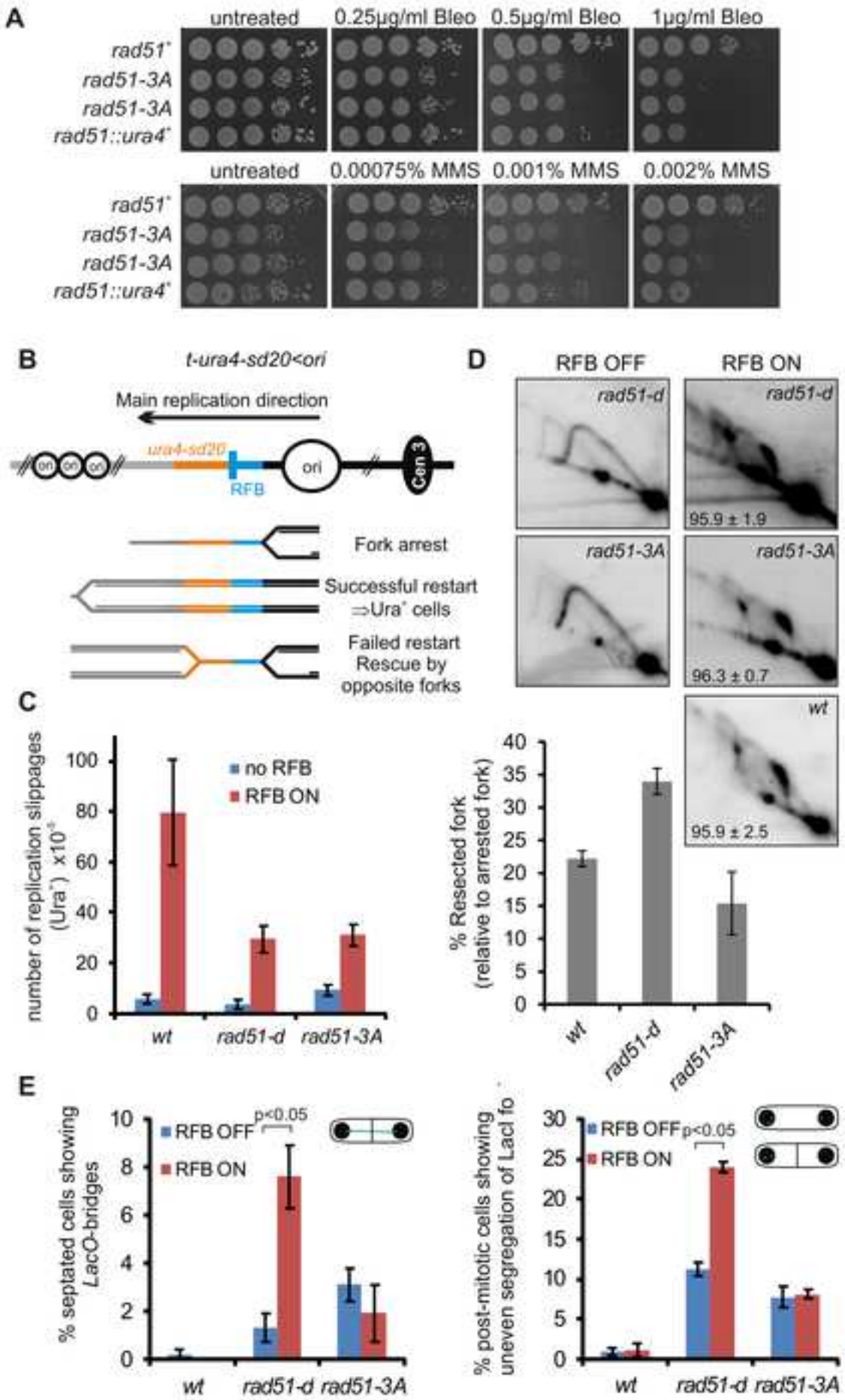
A
untreated
0.25µg/ml Bleo
0.5µg/ml Bleo
1µg/ml Bleo
rad51+
rad51-3A
rad51-3A
rad51::ura4+
untreated
0.00075% MMS
0.001% MMS
0.002% MMS
rad51+
rad51-3A
rad51-3A
rad51::ura4+
B
t-ura4-sd20<ori
Main replication direction
ori
ori
ori
ura4-sd20
RFB
ori
Cen 3
Fork arrest
Successful restart
⇒Ura+ cells
Failed restart
Rescue by
opposite forks
C
number of replication slippages
(Ura+) x10-5
no RFB
RFB ON
wt
rad51-d
rad51-3A
D
RFB OFF
RFB ON
rad51-d
rad51-d
95.9 ± 1.9
rad51-3A
rad51-3A
96.3 ± 0.7
wt
95.9 ± 2.5
% Resected fork
(relative to arrested fork)
wt
rad51-d
rad51-3A
E
% septated cells showing
LacO-bridges
RFB OFF
RFB ON
p<0.05
wt
rad51-d
rad51-3A
% post-mitotic cells showing
uneven segregation of LacI fo
RFB OFF
RFB ON
p<0.05
wt
rad51-d
rad51-3A

Figure7

Click here to download Figure ait-saada et al Figure 7.tif

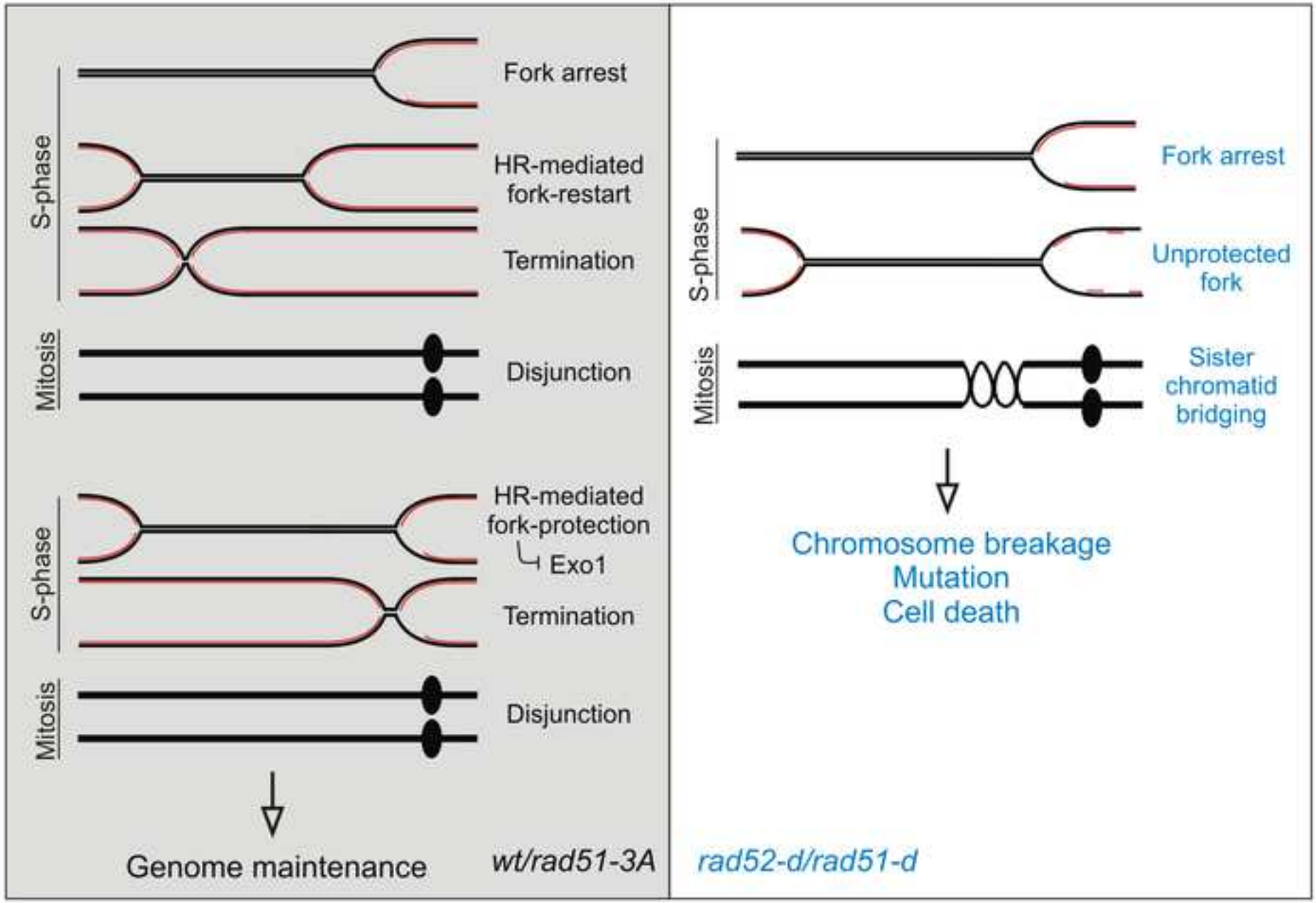

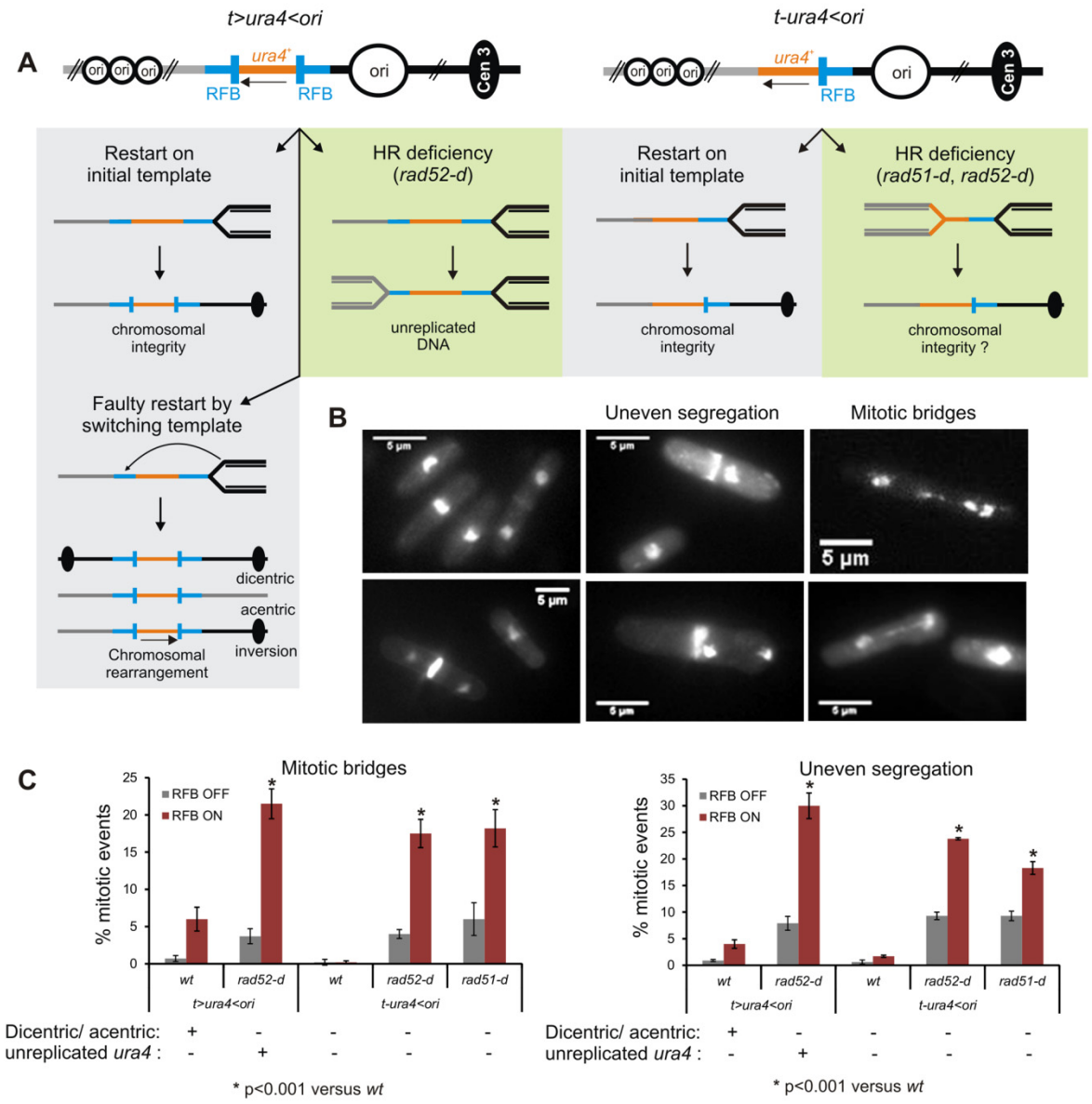

Figure S1: A single dysfunctional replication fork is sufficient to induce mitotic abnormalities in the absence of homologous recombination (related to Figure 1).

A. Diagram of the *t>ura4<ori* construct containing two *RTS1*-RFBs (> and <, blue bars) blocking the progression of forks converging towards the *ura4* locus (red bars), and of the *t-ura4<ori* construct containing a single *RTS1*-RFB (<, blue bars), which blocks the progression of replication forks moving in the main replication direction. At the *t>ura4<ori* locus (left panel), replication restart occurs either on the initial template or through a faulty template switch of nascent strands initiating DNA synthesis on a non-contiguous template (Lambert et al. Mol Cell 2010). Faulty template restart results in abnormal chromosomal structures, such as acentric and dicentric isochromosomes and inversion of the *ura4* marker. In cells defective for homologous recombination (HR deficiency), converging forks are blocked and not restarted, resulting in the *ura4* marker remaining unreplicated. At the *t-ura4<ori* locus (right panel), replication restart occurs on the initial template. In HR-deficient cells, the blocked fork is left irreversibly arrested.

B. Examples mitotic abnormalities observed with Dapi staining.

C. Quantification mitotic abnormalities observed in the strains and conditions indicated. For each genetic condition, it is indicated if acentric/dicentric chromosomes are expected to form (+) or not (-), and if the *ura4* gene is expected to be left unreplicated (+) or not (-). Strains used: for *t>ura4<ori*, *wt*=SL337, *rad52-d*=SL363; for *t-ura4<ori*, *wt*=SL350, *rad52-d*=SL680, *rad51-d*=SL395.

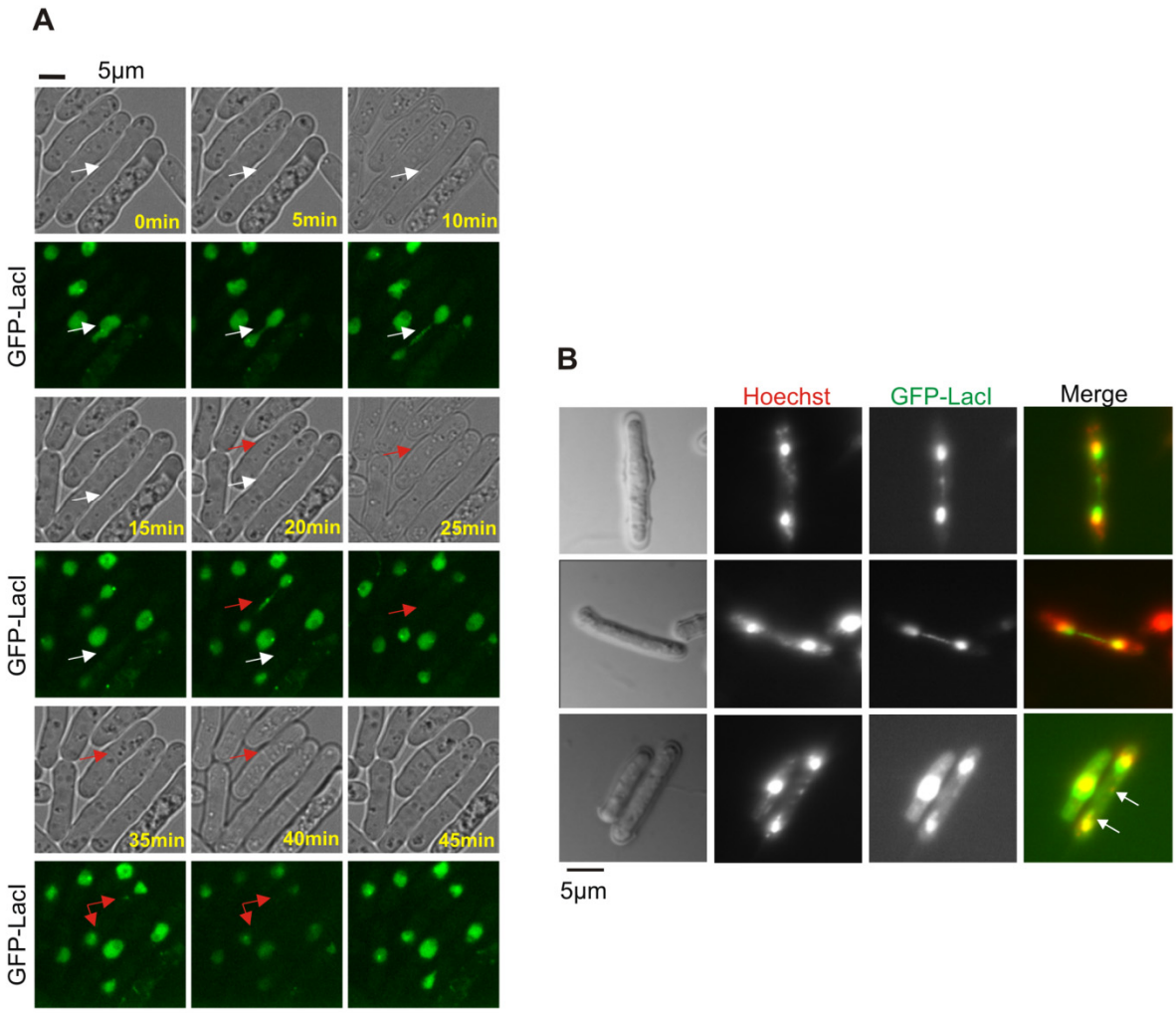

Figure S2: Examples of *LacO*-bridges and DNA staining (related to Figure 2)

A. Examples of *LacO*-bridges. Tracking of individual *LacO*-bridges in *rad52-d* cells from time-lapse movies: example of *LacO*-bridges resolved before cytokinesis, with (red arrow) and without (white arrow) breakage. Strain used: *rad52-d*=AA1.

B. Examples of Hoechst-negative stretched *LacO*-bridges (top and middle panel) and Hoechst-positive and broken *LacO*-bridges (Bottom panel). The white arrows indicate the part of the broken *LacO*-bridge positively stained with Hoechst. Strain used: *rad52-d*=AA1.

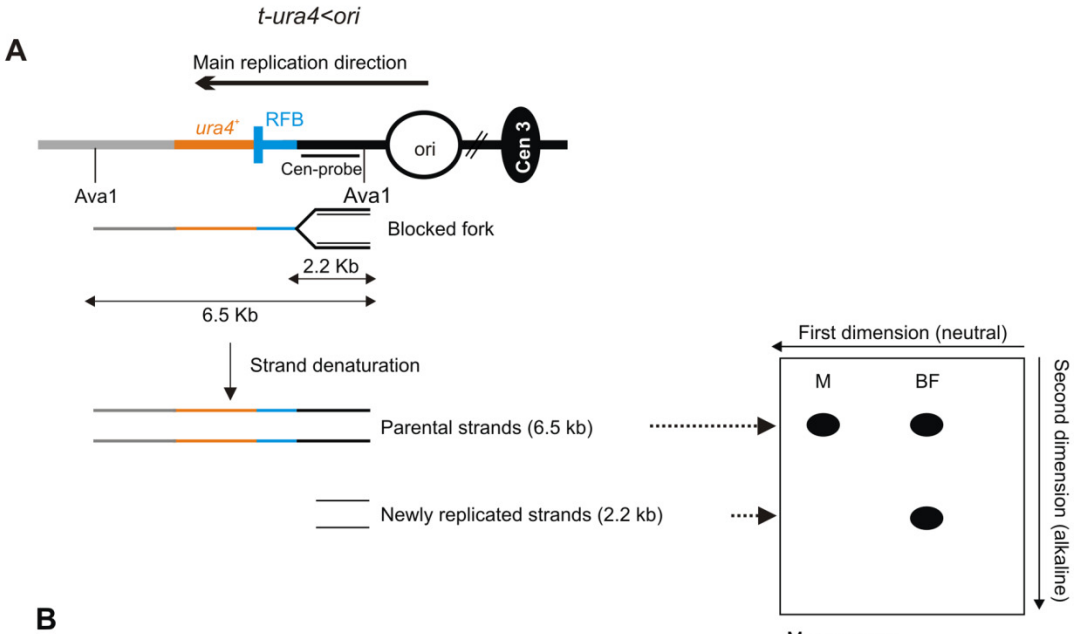

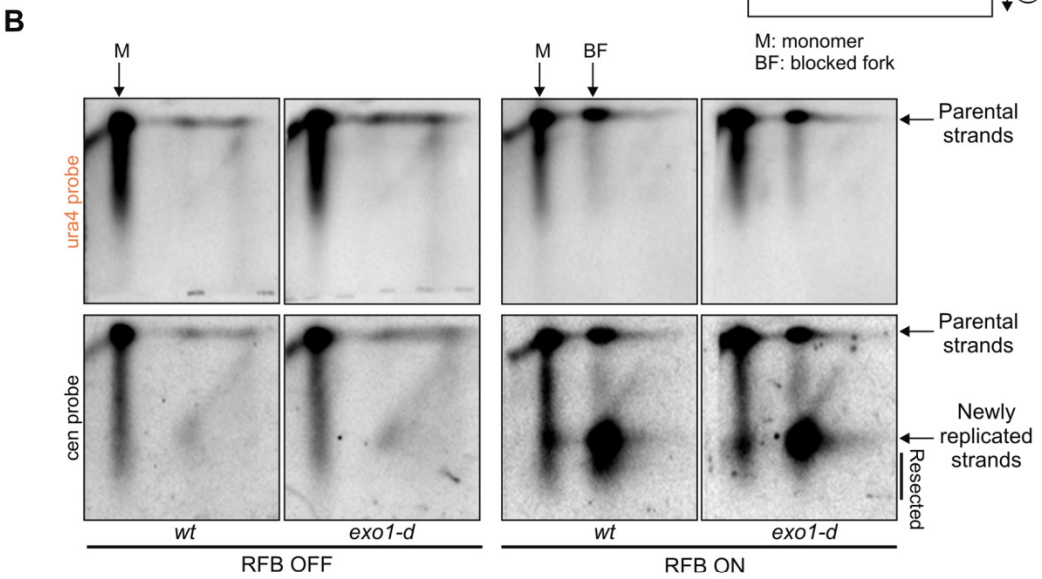

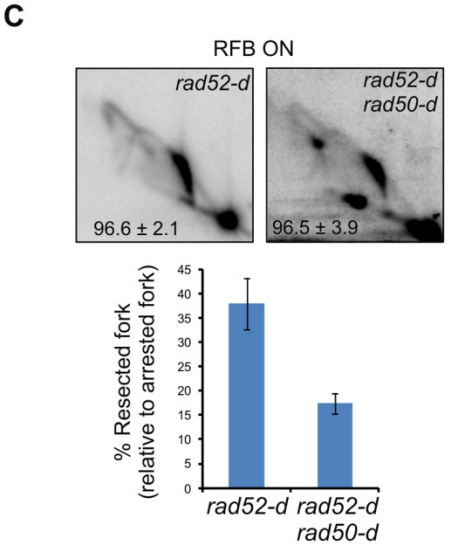

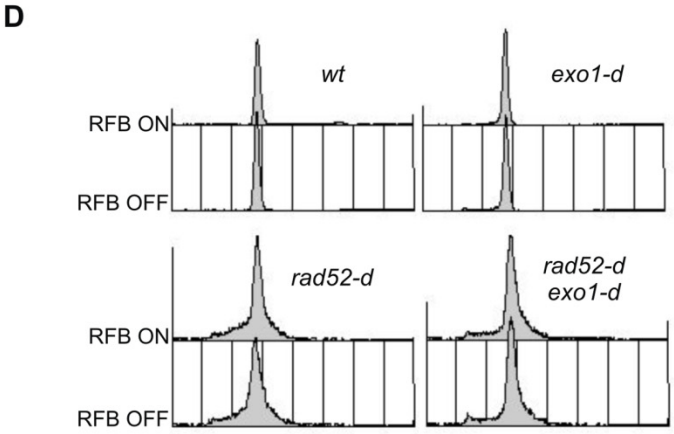

% mitotic cells	*rad52-d*	*exo1-d*	*rad52-d exo1-d*
RFB OFF	2.1	2.1	2.4
RFB ON	2	1.3	2.3

Figure S3: unprotected terminally-arrested forks contain newly replicated strands undergoing Exo1-mediated degradation (related to Figure 3 and 5)

A. Diagram of the *t-ura4<ori* containing a single *RTS1*-RFB (<, blue bars) blocking the progression of replication forks moving in the main replication direction, from the centromere towards the telomere. The locations of *Ava*1 restriction sites are indicated on the figure. Newly replicated strands at the active *RTS1*-RFB are 2.2 kb long, whereas the parental strands are 6.5 kb long. Electrophoresis was performed in neutral conditions in the first dimension, making it possible to separate the monomer (M, 6.5 kb) from the blocked fork (BF, 8.7 kb). The second dimension was performed in alkaline conditions, allowing the separation of parental strands from newly replicated strands, with discrimination on the basis of size.

B. Example of neutral-alkaline 2DGE at the active (RFB ON) or inactive (RFB OFF) *RST1*-RFB in the strains indicated. Hybridization with the ura4-probe detected no newly replicated strands, as expected, whereas hybridization with the cen-probe revealed newly replicated strands forming a smear indicating that they had been resected in an Exo1-dependent manner. Strains used: *wt*=YC13, *exo1-d*=II258.

C. Top panel: Representative RI analysis by 2DGE in the *rad50-d rad52-d* mutant in the absence (RFB OFF) or presence of fork blockade (RFB ON). A DNA fragment corresponding to the *ura4* gene was used as the probe. Numbers indicate the efficiency of the *RTS1*-RFB. Values correspond to the mean of at least three independent experiments ± standard deviation (SD).

Bottom panel: Quantification of % of fork undergoing resection (tail signals) relative to the number of blocked forks, in the strains indicated. The values shown are the means of at least three independent experiments ± the 99% confidence interval (99% CI). Strains used: *rad52-d*=YC90, *rad50-d rad52-d*=SL817.

D. Top panel: cell cycle distribution analyzed by FACS in indicated strains and conditions. Bottom panel: % of mitotic cells in indicated strains and conditions in an asynchronous population. Strains used: *wt*=AA23, *rad52-d*=AA1, *exo1-d*=AA39, *rad52-d exo1-d*=AA42. (related to Figure 5).

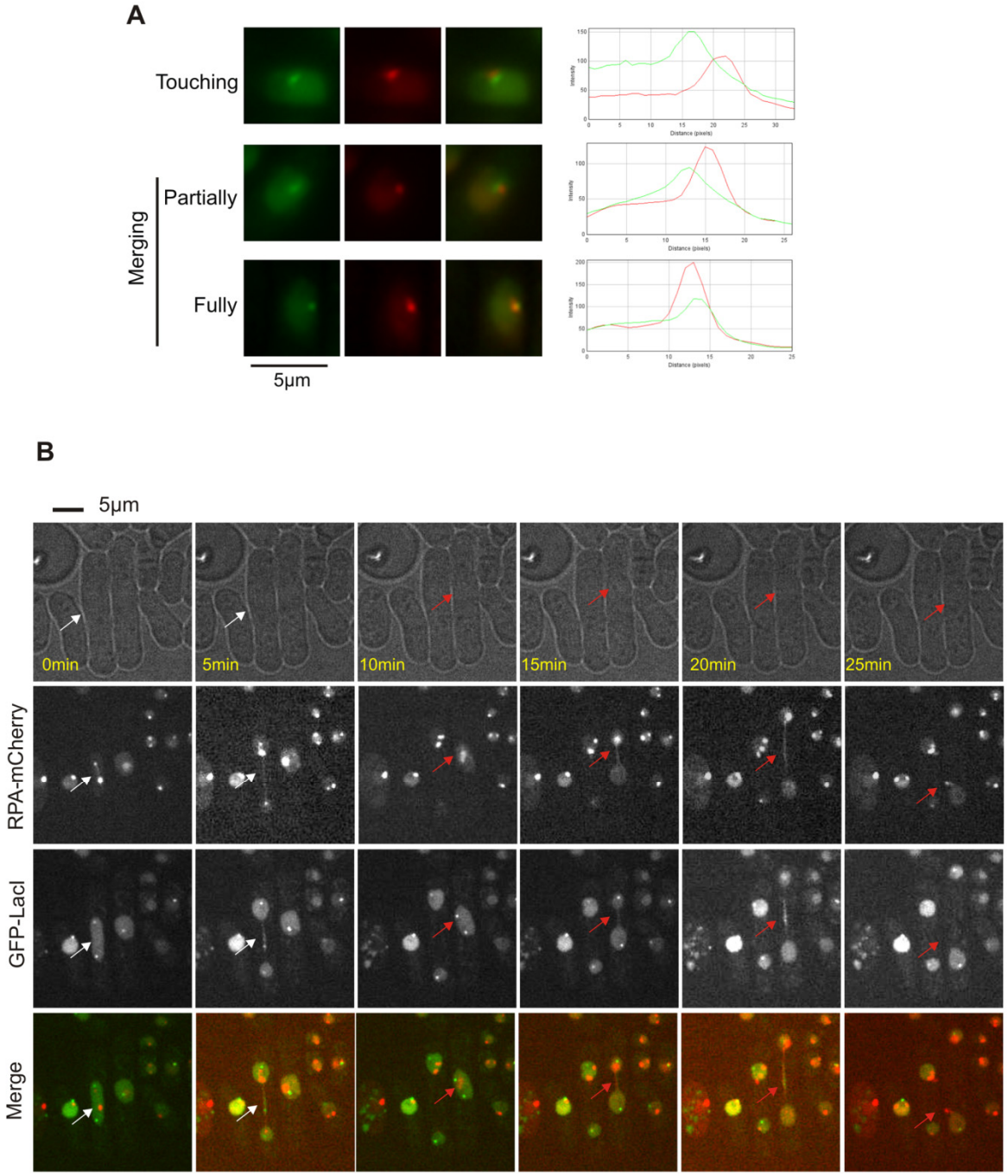

Figure S4: Examples of RPA focus co-recruited to the *RTS1*-RFB and RPA-positive *LacO*-bridges (related to Figure 4)

A. Examples of RPA focus touching/merging a GFP-LacI focus, with the respective line scans analysis done with image J. Top panel: Example of a RPA focus touching a GFP-LacI focus in the same Z-stack. Middle: Example of a RPA focus partially merging with a GFP-LacI focus in the same Z-stack. Bottom panel: Example of a RPA focus fully merging with a GFP-LacI focus in the same Z-stack.

B. Tracking of individual RPA-positive *LacO*-bridges in *rad52-d* cells from time-lapse movies. Examples of RPA-coated intertwined sister chromatid. White and red arrows represent two distinct events.

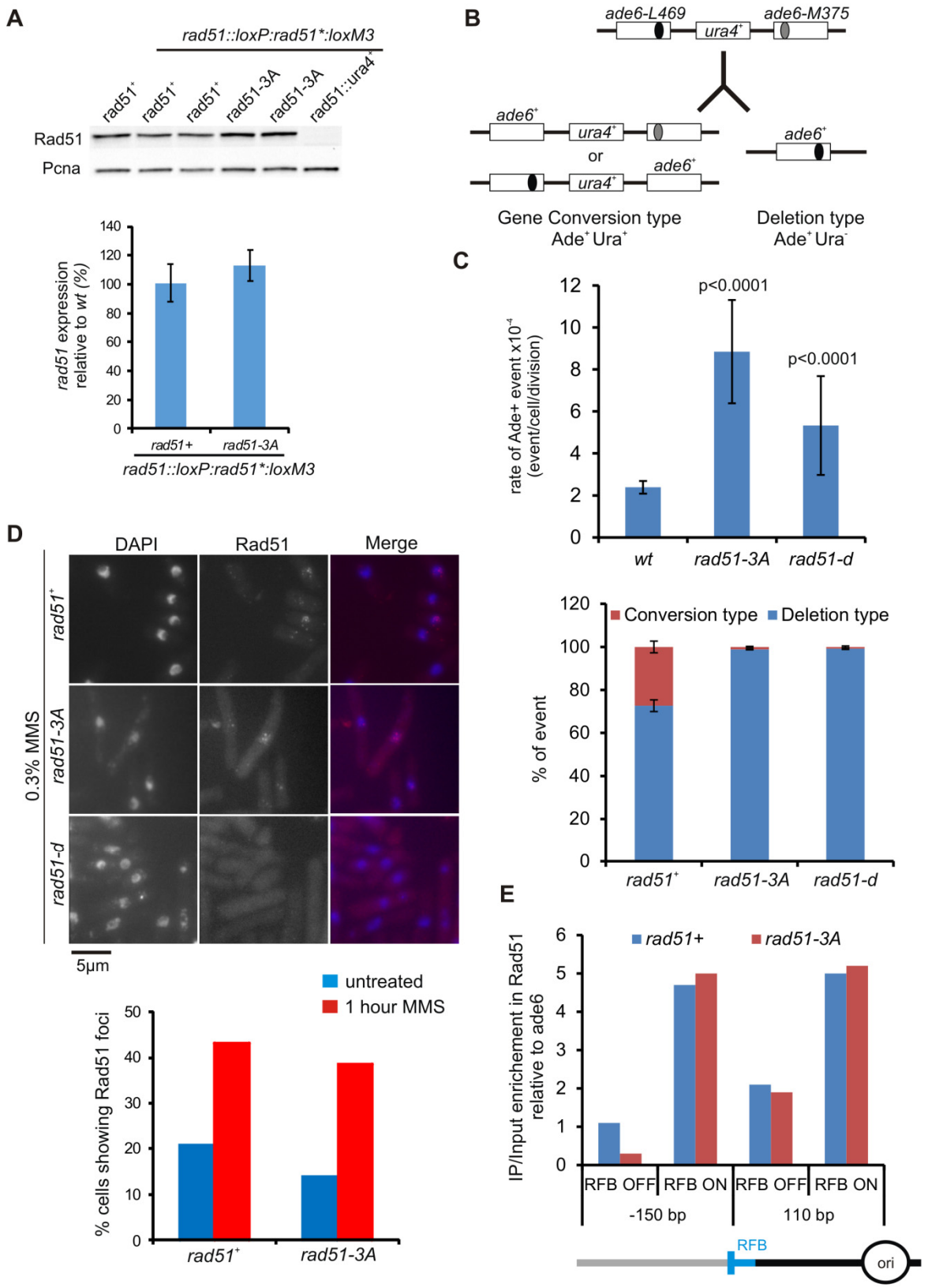

Extended Data Figure 5: Characterization of the *rad51-3A* mutant (related to Figure 6)

A. Top panel: expression of *wt* and mutated forms of Rad51 (*rad51-3A*) by immunoblotting with an anti-Rad51 antibody. For integration of the *rad51-3A* allele, the *rad51*$^{+}$ gene was first replaced with a *ura4*$^{+}$ marker flanked by loxP and loxM3 sites (*rad51::loxP:ura4:loxM3*) (Watson et al. Gene 2008).

Upon expression of the site-specific Cre recombinase, the *ura4*$^{+}$ marker was replaced by either the *rad51*$^{+}$ or *rad51-3A* allele, generating the following strains: *rad51::loxP:rad51:loxM3* and *rad51::loxP:rad51-3A:loxM3*. Two independent clones were tested for each genotype. Bottom panel: quantification of Rad51 levels in the strains indicated, normalized with respect to PCNA levels. The values shown are the means of four experiments ± the 95%CI. Strains used: *wt*=AA109, *rad51-3A*=AA118, *rad51-d*=SL1010.

B. Diagram of the direct *ade6* repeats used to monitor spontaneous recombination. Gene conversion events result in Ade+ Ura+ cells whereas deletion events result in Ade+ Ura- cells.

C. Top panel: Rate of Ade+ colony (event/cell/division) in indicated strains. Values are the median rate ± 95 CI. For each strain, 11-15 independent colonies grown on non-selective media (YEA) were re-suspended in water. Appropriate dilutions were plated on selective media (EMM –-Ade and EMM –Ade -Ura) and non-selective media to score viability. Colonies were counted after 5-7 days of incubation at 30°C. Each fluctuation test was repeated two times. Statistical analysis was performed with the Mann-Whitney U test. Bottom panel: % of deletion (Ade+ Ura-) and conversion type (Ade+ Ura+) in indicated strains. Strains used: *wt*=AA223, *rad51-3A*=AA237, *rad51-d*=AA241.

D. Top panel: examples of Rad51 foci detected by immunofluorescence, using an anti-Rad51 antibody, in indicated strains. The *rad51-d* strain was used as control of antibody specificity. Cells were treated for 1 hour with 0.3 % MMS. Bottom panel: quantification of Rad51 foci in indicated strains and conditions. Strains used: *wt*=AA109, *rad51-3A*=AA118, *rad51-d*=SL1010.

E. Recruitment of Rad51 to the *RTS1*-RFB, 150 bp downstream the RFB and 110bp upstream the RFB, in indicated strains and conditions. Strains used: *wt*=AA129*, rad51-3A*=AA133.

Table S1: Strains used in this study (related to Key resources table of the STAR method section).

Strain number		*Genotype*	*Reference*
SL337	*h-smt0*	*t>ura4^{+}<ori rtf1:nmt41:sup35 ade6-704 leu1-32*	*Lambert et al. 2005*
SL350	*h-smt0*	*t-ura4^{+}<ori (uraR) rtf1:nmt41:sup35 ade6-704 leu1-32*	*Lambert et al. 2005*
SL363	*h-smt0*	*rad52::Kan t>ura4^{+}<ori rtf1:nmt41:sup35 ade6-704 leu1-32*	*Lambert et al. 2005*
SL680	*h-smt0*	*Rad52::Kan t-ura4^{+}<ori (uraR) rtf1:nmt41:sup35 ade6-704 leu1-32*	*Lambert et al. 2010*
SL382	*h+*	*Rad51 ::Kan t>ura4^{+}<ori (RuraR) rtf1:nmt41:sup35 ade6-704 leu1-32*	*Lambert et al. 2010*
SL395	*h+*	*Rad51 ::Kan t-ura4^{+}<ori (uraR) rtf1:nmt41:sup35 ade6-704 leu1-32*	*Lambert et al. 2010*
AA23	*h-smt0*	*arg3::psv40-GFP-LacI** LacO 7,9Kb:kan t-ura4^{+}<ori nmt41:rtf1:sup35 ade6-704 leu1-32*	*This study*
AA1	*h-smt0*	*rad52::nat arg3::psv40-GFP-LacI** LacO 7,9Kb:kan t-ura4^{+}<ori nmt41:rtf1:sup35 ade6-704 leu1-32*	*This study*
YC219	*h+*	*ssb3:YFP:Nat rtf1:nmt41:sup35 t<ura4-SD20-ori ade6-704 leu1-32*	*This study*
YC223	*h+*	*ssb3:YFP:Nat rad52::Nat rtf1:nmt41:sup35 t<ura4-SD20-ori ade6-704 leu1-32*	*This study*
YC221	*h+*	*ssb3:YFP:Nat exo1::Nat rtf1:nmt41:sup35 t<ura4-SD20-ori ade6-704 leu1-32*	*This study*
AC434	*h+*	*ssb3:YFP:Nat rad52::Kan exo1::Nat rtf1:nmt41:sup35 t<ura4-SD20-ori ade6-704 leu1-32*	*This study*
YC13	*h-smt0*	*t-ura4-SD20<ori rtf1:nmt41:sup35 ade6-704 leu1-32*	*Iraqui et al. 2012*
YC90	*h-smt0*	*rad52::Nat t-ura4-SD20<ori rtf1:nmt41:sup35 ade6-704 leu1-32*	*Iraqui et al. 2012*
II258	*h-*	*exo1::Nat t-ura4-SD20<ori rtf1:nmt41:sup35 ade6-704 leu1-32*	*Iraqui et al. 2012*
AA15	*h+*	*rad52::Nat exo1::Nat t-ura4-SD20<ori rtf1:nmt41:sup35 ade6-704 leu1-32*	*This study*
SL817	*h-smt0*	*rad52::Nat rad50::kan t-ura4-SD20<ori rtf1:nmt41:sup35 ade6-704 leu1-32*	*This study*
AS39	*h+*	*arg3::psv40-GFP-LacI** ssb3-mCherry:kan LacO 7,9Kb:kan t-ura4^{+}<ori nmt41:rtf1:sup35 ade6-704 leu1-32*	*This study*
SL1190	*h-smt0*	*rad52::nat ssb3-mCherry:kan arg3::psv40-GFP-LacI** ssb3-mCherry:kan LacO 7,9Kb:kan t-ura4^{+}<ori nmt41:rtf1:sup35 ade6-704 leu1-32*	*This study*
AA46	*h+*	*exo1::hygro ssb3-mCherry:kan arg3::psv40-GFP-LacI** ssb3-mCherry:kan LacO 7,9Kb:kan t-ura4^{+}<ori nmt41:rtf1:sup35 ade6-704 leu1-32*	*This study*
SL1194	*h-smt0*	*rad52::nat exo1::hygro ssb3-mCherry:kan arg3::psv40-GFP-LacI** ssb3-mCherry:kan LacO 7,9Kb:kan t-ura4^{+}<ori nmt41:rtf1:sup35 ade6-704 leu1-32*	*This study*
AA39	*h+*	*exo1::hygro arg3::psv40-GFP-LacI** LacO 7,9Kb:kan t-ura4^{+}<ori nmt41:rtf1:sup35 ade6-704 leu1-32*	*This study*
AA42	*h-smt0*	*rad52::nat exo1::hygro arg3::psv40-GFP-LacI** LacO 7,9Kb:kan t-ura4^{+}<ori nmt41:rtf1:sup35 ade6-704 leu1-32*	*This study*
SL504	h+	*rtf:nmt41:sup35 t<ura4^{+}-ori ade6-704 leu1-32*	*Iraqui et al. 2012*
AA91	*h-smt0*	*rad52::kan rtf:nmt41:sup35 t<ura4^{+}-ori ade6-704 leu1-32*	*This study*
AA95	*h-smt0*	*exo1::nat rtf:nmt41:sup35 t<ura4^{+}-ori ade6-704 leu1-32*	*This study*
AA98	*h-smt0*	*rad52::kan exo1::nat rtf:nmt41:sup35 t<ura4^{+}-ori ade6-704 leu1-32*	*This study*

YC266	*h-*	*rtf1:nmt41:sup35 ade6-704 ura5::hygro t-13xter-ura4SD20-ura5<ori leu1-32*	*This study*
II558	*h+*	*rad52::kan rtf1:nmt41:sup35 ade6-704 ura5::hygro t-13xter-ura4SD20-ura5<ori leu1-32*	*This study*
YC270	*h+*	*exo1::nat rtf1:nmt41:sup35 ade6-704 ura5::hygro t-13xter-ura4SD20-ura5<ori leu1-32*	*This study*
YC274	*h+*	*rad52::kan exo1::nat rtf1:nmt41:sup35 ade6-704 ura5::hygro t-13xter-ura4SD20-ura5<ori leu1-32*	*This study*
AA109	*h+*	*loxP:rad51^{+}:LoxM3 ura4-D18 ade6-704 leu1-32*	*This study*
AA118	*h+*	*loxP:rad51 R152A-R324A- K334A:LoxM3 (rad51-3A) ura4-D18 ade6-704 leu1-32*	*This study*
SL1010	*h+*	*rad51::loxP:ura4+:loxM3 ura4-D18ade6-704 leu1-32*	*This study*
AA124	*h-smt0*	*loxP:rad51^{+}:LoxM3 t-ura4-SD20-ori rtf1:nmt41:sup35 ade6-704 leu1-32*	*This study*
AA129	*h-smt0*	*loxP:rad51^{+}:LoxM3 t-ura4-SD20<ori rtf1:nmt41:sup35 ade6-704 leu1-32*	*This study*
YC76	*h-smt0*	*Rad51::Kan t-ura4-SD20-ori rtf1:nmt41:sup35 ade6-704 leu1-32*	*Iraqui et al. 2012*
YC80	*h-smt0*	*Rad51::Kan t-ura4-SD20<ori rtf1:nmt41:sup35 ade6-704 leu1-32*	*Iraqui et al. 2012*
AA133	*h-smt0*	*loxP:rad51 R152A-R324A- K334A:LoxM3 (rad51-3A) t-ura4-SD20<ori rtf1:nmt41:sup35 ade6-704 leu1-32*	*This study*
AA139	*h-smt0*	*loxP:rad51 R152A-R324A- K334A:LoxM3 (rad51-3A) t-ura4-SD20-ori rtf1:nmt41:sup35 ade6-704 leu1-32*	*This study*
AA158	*h+*	*loxP:rad51 R152A-R324A-K334A:LoxM3(rad51-3A) arg3::psv40-GFP-LacI** LacO 7,9Kb:kan t-ura4^{+}<ori nmt41:rtf1:sup35 ade6-704 leu1-32*	*This study*
AC409	*h-smt0*	*rad51::kan trp2::psv40-GFP-LacI** LacO 7,9Kb:kan t-ura4^{+}<ori nmt41:rtf1:sup35 ade6-704 leu1-32*	*This study*
AA223	*h-smt0*	*loxP:rad51+:loxM3 ade6M-375int:puc8/ura4+/ade6-469 ura4D18 leu+*	*This study*
AA237	*h-smt0*	*loxP:rad51-3A:loxM3 ade6M-375int:puc8/ura4+/ade6-469 ura4D18 leu+*	*This study*
AA241	*h-smt0*	*rad51::kan ade6M-375int:puc8/ura4+/ade6469 ura4D18 leu+*	*This study*

Table S2: Primers used in this study (related to Key resources table of the STAR method section).

Name	Distance (pb) from the *RTS1*-RFB position	Sequence (5'-3')	Experiment
L3F	110	TTTAAATCAAATCTTCCATGCG	ssDNA qPCR
L3R		TGTACCCATGAGCAAACTGC	ssDNA qPCR
L400F	450	ATCTGACATGGCATTCCTCA	ssDNA qPCR
L400R		GATGCCAGACCGTAATGACA	ssDNA qPCR
L1800F	1800	GGCAAAGTAGATCCGACAGC	ssDNA qPCR
L1800R		TGAATACGCCGTTACTCCTAAAG	ssDNA qPCR
L2200F	2200	AAGGCAAGAAACGCTGAGAC	ssDNA qPCR
L2200R		GGCATGCATACTACCCGATAA	ssDNA qPCR
II50F	Locus control (ChrII)	CACCGCAGTTCTACGTATCCT	ssDNA qPCR
II50R		CGATGTAACGGTATGCGGTA	ssDNA qPCR
II150F	Chromosome II	ATCGTCAATCCATTCCGTCT	ssDNA qPCR
II150R		AACCATCTAACATACGATATGAATCCT	ssDNA qPCR
R1800F	-1800	TTACATTGCTCAATGCTGACG	ChIP RPA
R1800R		AACGTGGTAGTACGACAAGGTACA	ChIP RPA
Ura4-1F	-1100	GACTCCACGACCAACAATGA	ChIP RPA
Ura4-1R		CTGGTATCGGCTTGGATGTT	ChIP RPA
R400F	-600	CACACTTGCTCTGTACACGTATTCT	ChIP RPA
R400R		AGGATCCATGATGCACAGATT	ChIP RPA
R5F	-210	TTGCCAAACATCCTCCTACC	ChIP RPA
R5R		GAAACACAAGCCAAAGTTGC	ChIP RPA
R3F	160	TTCTGTTCCAACACCAATGTTT	ChIP RPA
R3R		TGTACAAAGCCAATGAAAGATG	ChIP RPA
Ura4-1F	600	GACTCCACGACCAACAATGA	ChIP RPA
Ura4-1R		CTGGTATCGGCTTGGATGTT	ChIP RPA
Ura4-2F	950	TGATATGAGCCCAAGAAGCA	ChIP RPA
Ura4-2R		CAAATTCGCAGACATTGGAA	ChIP RPA
L5F	1500	AGGGCATTAAGGCTTATTTACAGA	ChIP RPA
L5R		TCACGTTTAATTTCAAACATCCA	ChIP RPA
L3F	1850	TTTAAATCAAATCTTCCATGCG	ChIP RPA
L3R		TGTACCCATGAGCAAACTGC	ChIP RPA
L400F	2200	ATCTGACATGGCATTCCTCA	ChIP RPA
L400R		GATGCCAGACCGTAATGACA	ChIP RPA
L600F	2500	CCATTGACTAGGAGGACTTTGAG	ChIP RPA
L600R		CCCTGGCGGTTGTAGTTAGT	ChIP RPA
L1400F	3100	AACATCGGTGACCTCGTTCT	ChIP RPA
L1400R		CTCTTCGCTCCAAGCGTTAT	ChIP RPA
Ade6-23	Chromosome III	GGCTGCCTCTACCATCATTC	ChIP RPA
Ade6-25		TTAAGCTGAGCTGCCAAGGT	ChIP RPA